The effect of microstructure on the permeability of metal foams

Virendra Loya

A Thesis

In

The Department

Of

Mechanical and Industrial Engineering

Presented in Partial Fulfillment of the Requirements

for the Degree of Master of Applied Science at

Concordia University

Montréal, Québec, Canada

July 2005

ABSTRACT

The effect of microstructure on the permeability of metal foams

Virendra Loya

Metal foam (MF) is a superior material with complex structure made from different kinds of materials manufactured using novel technology. Due to its several unique properties with high porosity and high surface area, it finds use in wide area of engineering, such as energy absorbers, filters, heat exchangers etc. The structures of metal foam are very intricate and irregular and it is very difficult to accurately predict the impact of microstructure on pressure drop. Most of the recent literature studied permeability at low velocity range. Thus the present study was carried out to have better understanding of permeability for greater velocity range to suit industrial applications. The necessary equipment was designed and built for this purpose. Pressure drop across the metal foams was measured on IMI metal foam (IMIMF) and ReceMat metal foam (RMF) samples. Darcian and non-Darcian permeability parameters, K and C, were determined by fitting experimental data with widely accepted quadratic model of Hazen-Dupuit-Darcy at different velocity ranges. Generally, the experimental results are in good agreement with the model with correlation coefficient, R^2, higher than 98 %. For IMI samples, pore size and window size were measured through SEM and image analysis. The permeability K is significantly affected by pore size and porosity. For both foams, as the porosity increases, pressure drop decreases or permeability, K, increases, but the optimum porosity that corresponds to the maximum permeability could not be found. The pressure drop observed in the metal foams is due to combined effect of K and C. Nevertheless, the introduction of the open cross sectional area term enabled better understanding of the

permeability of intricate morphologies like IMIMF. Whereas, K and C could be predicted by Ergun-like model in simple and homogenous structure of RMF using appropriate value for empirical constants *A* and *B*. Quadratic term of Hazen-Dupuit-Darcy equation is found to be due to inertia of the flowing fluid and may be due to drag exerted by the microstructure of the porous media.

ACKNOWLEDGEMENTS

The author is sincerely thankful to his supervisor Dr. Mamoun Medraj because he has been the backbone for me accomplishing the hardest task I ever endured here at Concordia University. He is an excellent instructor who provided me with knowledge, enthusiastic guidance, advice and continuous support. During the course of this work, sometimes I felt stalemate like situation but I am grateful to him that he drove me out of that.

I am very thankful to the researchers at IMI, Boucherville, Louise-Philippe Lefebvre, Eric Baril and Maxime Gauthier for their guidance, timely assistance to use the facilities at IMI and providing me with the materials that I used throughout my experiment. I would like to give my sincere thanks to Mr. H. S. Verduyn (from RECEMAT International) for providing the samples.

I would like to thank the administrative and technical support staff in Mechanical and Industrial Engineering Department, John Elliot, Brain Cooper, Brad Luckhart and Gilles Huard.

Thanks also to my colleagues and friends for their help and useful discussions during course of work.

Finally I would like to express my deepest gratitude to my parents, wife and sister for their unwavering strength and continuous moral support throughout the research period.

TABLE OF CONTENTS

CHAPTER 5

LIST OF FIGURES

LIST OF TABLES

CHAPTER 1

1.1 INTRODUCTION

In the past few years, there has been a considerable increase in interest for metal foams, especially made of aluminum or aluminum alloys. The reasons for this are recent process developments, which provide a better quality of the foamed material. Moreover, the conditions for the application of new materials have changed very much. Increased demands concerning passenger safety in automobiles or materials recycling make constructors now think of using metal foams where a few years ago the same material would have been ruled out for technical or economic reasons. Metal foams were characterized by relatively high costs and a poor quality of the foamed material [1]. In the last 10 years, there has been quite some improvement in these aspects, so that currently various methods for making metal foams are available, some starting from the molten metal and others from metal powders. In particular, a powder method for foaming metals was invented a few years ago. It allows for the production of foamed metals based on aluminum, zinc, tin, lead and their alloys. There are many possible applications for metal foams ranging from light-weight construction, sound and heat insulation to energy absorption and implants in biomedical applications. The latter makes use of the combination of high strength and the non-linear deformation behavior which originates from the cellular nature of metal foams [2].

Metal foam is one of the recent developments in material science and hence so far not studied in depth. Currently, metal foam properties like heat conduction, permeability, deformation behavior are common research areas [1]. Out of these, research on permeability of metal foam is discussed in greater detail in this thesis.

1.2 Making of Metal Foams

There are several process-routes that have been developed to make metal foams. They fall into four broad classes:

- foams formed from the vapor phase;
- foams electrodeposited from an aqueous solution;
- foams which depend on liquid-state processing; and
- foams that are created in the solid state;

Each method can be used with a small subset of metals to create a porous material with a limited range of relative densities and cell sizes. Some produce open-cell foams, others produce foams in which the majority of the cells are closed [3].

The properties of metal foam and other cellular metal structures depend upon the properties of the metal, the relative density and cell topology (e.g. open or closed cell, cell size, etc.). Metal foams are made by one of the eight processes listed below; only the first five are commercialized and shall be discussed in this section. Most commercial metal foams available today are made of aluminum, but review of the recent patents shows the development of methods for foaming other light metals like magnesium and titanium as well as other common nonferrous or ferrous metals. The most recent developments shall be discussed at the end of this section.

1. Melt gas injection
2. Gas releasing particles decomposition in melt
3. Gas releasing particles decomposition in semisolids
4. Casting using a polymer or wax precursor as template
5. Metal deposition on cellular preforms

6. Entrapped gas expansion
7. Hollow sphere structure
8. Gas melt eutectic solidification

1.2.1 Melt Gas Injection

Pure liquid metals cannot easily be caused to foam by bubbling a gas into them. Drainage of liquid down the walls of the bubbles usually occurs too quickly preventing the foam from remaining stable long enough to solidify. However, 10-30% of small, insoluble, or slowly dissolving particles, such as aluminum oxide or silicon carbide, raises the viscosity of the aluminum melt and impedes drainage in the bubble membrane which, in turn, stabilizes the foam. There are several variants of the method, one of which is shown in Figure 1.1. Pure aluminum or an aluminum alloy is melted and 5-15 wt% of the stabilizing ceramic particles are added [2].

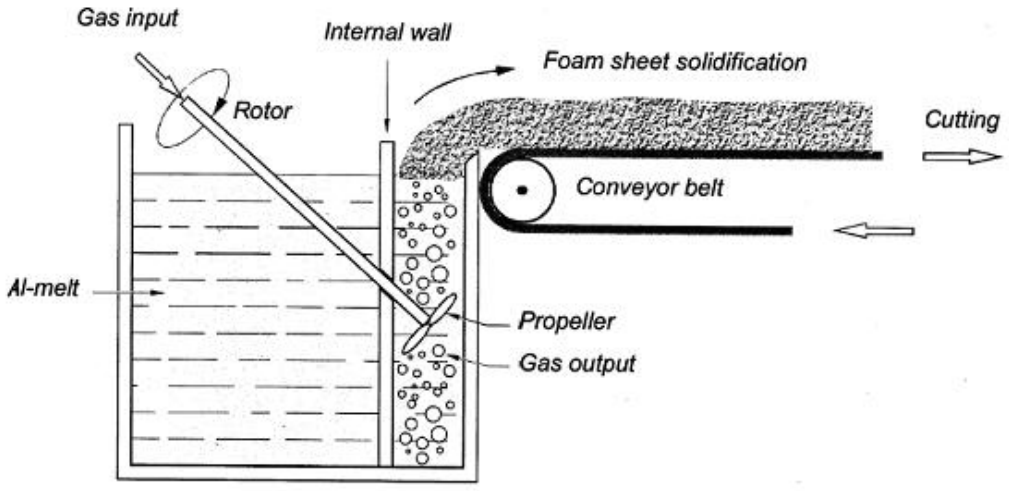

Figure 1.1: Manufacture of aluminum foam by the melt gas injection method [2].

These particles, typically 0.5-25μm in diameter, can be made of alumina, zirconia, silicon carbide, or titanium di-boride. A variety of gases can be used to create bubbles within liquid aluminum such as air, carbon dioxide, oxygen, inert gases and even water. Bubbles formed by this process float to the melt surface, drain and then begin to solidify. Low relative density with closed cell foams can be produced by carefully controlling the gas injection process and the cooling rate of the foam [3].

1.2.2 Gas-releasing particle decomposition in the melt

Metal alloys can be foamed by mixing into them a foaming agent that releases gas when heated. Figure 1.2 describes the process. The widely used foaming agents are titanium and zirconium hydrides (TiH_2 and ZrH_2). Other metal hydrides are Li, Na, K, Ru and Ce [4]. TiH_2 begins to decompose into Ti and gaseous H_2 when heated above 465°C which is well below the melting point of pure aluminum (660°C) and of its alloys. By adding TiH_2

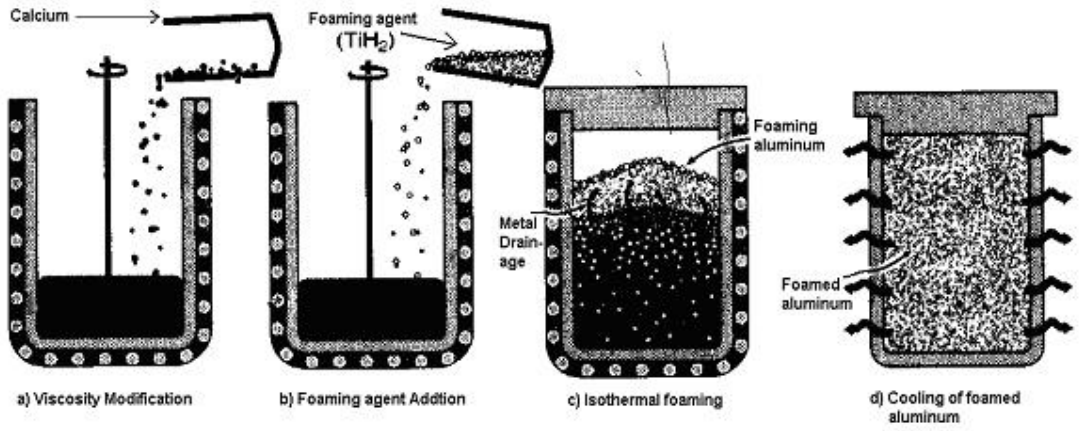

Figure 1.2: Manufacturing of aluminum foams by gas-releasing particle decomposition in the melt [3].

particles to an aluminum melt, large volumes of hydrogen gas are rapidly produced, creating bubbles that can lead to closed-cell foam. Its viscosity can be raised by adding 1-2% of calcium which rapidly oxidizes and forms finely dispersed CaO and $CaAl_2O_4$ particles. When foaming is complete, the melt is cooled to solidify the foam before the hydrogen escapes and the bubbles collapse [3]. The volume fraction of calcium and titanium hydride added to the melt ultimately determines the relative density and, in combination with cooling conditions, the cell size. The cell size can vary from 0.5 to 5 mm by changing the TiH_2 content, and the foaming and cooling conditions [2, 3].

1.2.3 Gas-releasing particle decomposition in semi-solids

This process is different from the previous process since foaming agents are introduced into metals in the solid state, instead of liquid state, by mixing and consolidating powders. A schematic diagram of the manufacturing sequence is shown in Figure 1.3.

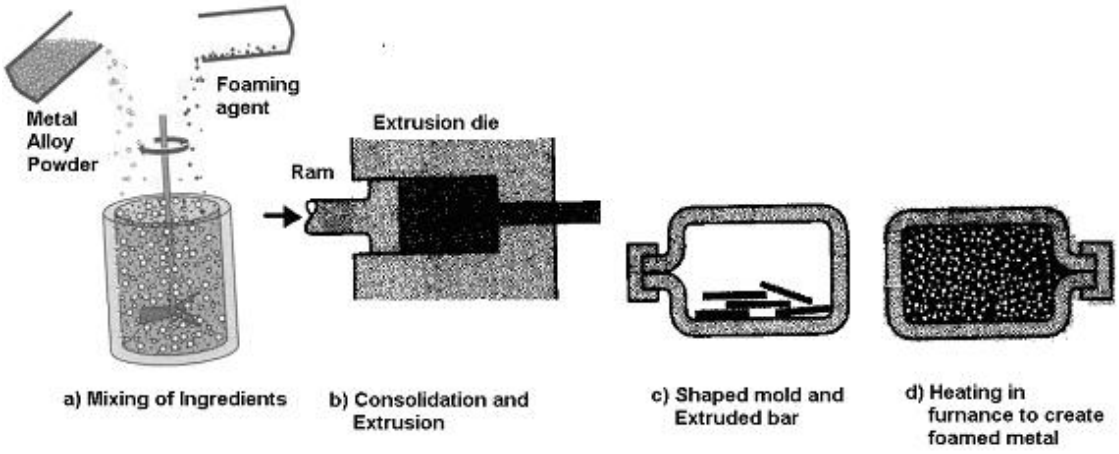

Figure 1.3: Powder metallurgy steps used to manufacturing metal foams by gas releasing particles in semi-solids [3].

It begins by combining particles of a foaming agent (TiH_2) with an aluminum alloy powder. After the ingredients are thoroughly mixed, the powder is cold compacted and then extruded into a bar or plate of near theoretical density. This 'precursor' material is chopped into small pieces, placed inside a sealed split mold and heated to a slightly above the solidus temperature of the alloy. Near net shaped parts can be obtained, this is done by inserting the precursor material into a hollow mold and expanding it by heating [2, 3].

1.2.4 Casting using a polymer or wax precursor as template

Open-cell polymer foams with low relative densities and a wide range of cell sizes of great uniformity are available from numerous sources. They can be used as templates to create investment-casting molds into which a variety of metals and their alloys can be cast. The method is schematically illustrated in Figure 1.4. An open-cell polymer foam

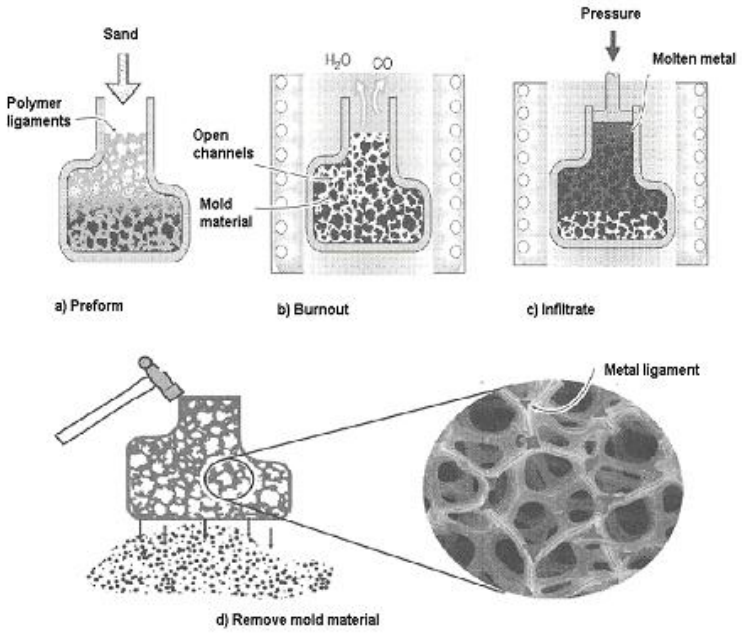

Figure 1.4: Investment casting method used to make open cell metal foams [3].

coated with a mold casting (ceramic powder) slurry, which is then dried and embedded in casting sand. The mold is then baked both to harden the casting material and to decompose (and evaporate) the polymer template, leaving behind a negative image of the foam. This mold is subsequently filled with a molten metal alloy and allowed to cool. After directional solidification and cooling, the mold materials are removed leaving behind the metal equivalent to the original polymer foam. The method gives open-cell foams with pore sizes of 1-5 mm and relative densities as low as 0.05. The process can be used to manufacture foams from almost any metal that can be investment cast. However major difficulty with this technique is the insufficient mechanical strength of the metal foam compared to the other available methods [2, 3].

1.2.5 Metal deposition on cellular preforms

Open-cell polymer foams can serve as templates upon which metals are deposited by chemical vapor decomposition (CVD), by evaporation or by electro-deposition. In the INCO process, nickel is deposited by the decomposition of nickel carbonyl, $Ni(CO)_4$ at 100°C. Infrared or RF (Radio Frequency) heating can be used to heat only the polymer foam. The metal-coated polymer foam is removed from the CVD reactor and the polymer is burnt out by heating in air. This results in a cellular metal structure with hollow ligaments. A subsequent sintering step is used to densify the ligaments. Nickel carbonyl gas is highly toxic and requires costly environmental controls. The method is restricted to pure elements such as nickel or titanium because of the difficulty of CVD or electro-deposition of alloys. It gives the lowest relative density (0.02 - 0.05) foams available today [3].

1.2.6 Recent developments in making metal foam

Review of the recent foam manufacturing patents shows improvements to the metal foam production process that provide better foaming control and improved metal foam properties. Recent European patent has successfully used biogel formers or bio binders. This method involves preparation of stable metallic or ceramic powder slurry comprising gelling agent. Gelling agent can be gelatine, agar, inulin, starch, potato dextrin etc. This slurry is then mixed with sacrificial material such as styrene seeds, nuts, peas, which can be later burnt out to get hollow shape. Choice is made depending on desired hollow shape like spheroid, ellipsoid etc. After mixing drying is carried out, a burn out step followed between 500°C to 600°C in which sacrificial material is burnt out, and sintering is then performed. This method gives good mechanical strength compared to casting using polymer method [5]. The same researchers have used biogel binder in metal foam produced by casting method depicted in Figure 1.5. Ceramic slurry, foaming agents and bio binders are mixed. During mixing gelation of the binders is prevented by continuously heating the mixture. Mixture is then allowed to cool in a mold (gelation) and then followed by thermal treatment. Thermal treatment involves calcinations and sintering steps at different temperature depending on the ceramic used [6]. A Japanese patent, however, has successfully foamed aluminum using a water based binder. The method involves an aqueous solution of a water soluble polymer (such as polyvinyl alcohol) that is mixed and kneaded with inorganic powder such as metal powder or ceramic powder. Next, oil materials such as paraffin wax and a surfactant (which are separated from water and solidified at around room temperature) are added and mixed. After that, the mixture is cast into a mold, and is freezed and solidified. Further, the wax

is dissolved and extracted by degreasing with supercritical carbon dioxide or through heating to produce a solidified body of foamed powder, which is subsequently sintered to produce foamed metal [7].

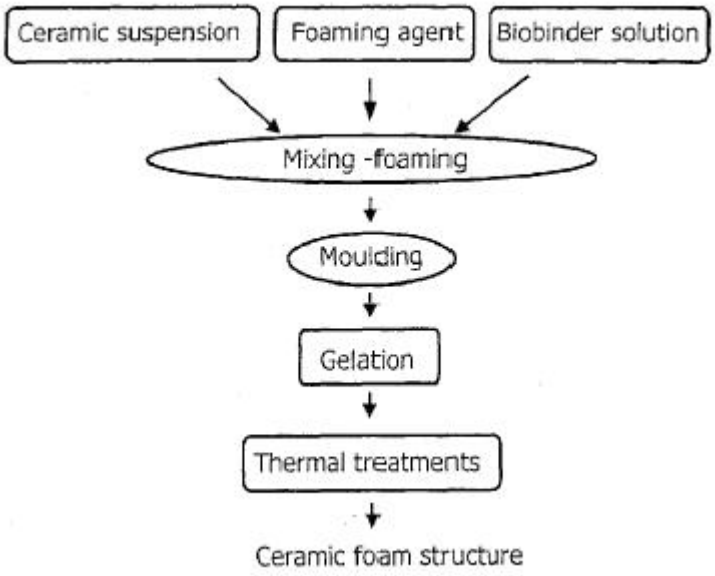

Figure 1.5: Method for producing foam by casting using biogel binder [6].

IMI (Industrial Metal Institute, Canada) has used polymer based binder to produce nickel foam. This procedure consists of forming polymer foams highly charged with metallic particles, eliminating the polymer by thermal decomposition and consolidating the particles by sintering. A metallic powder, a solid polymer binder (i.e. resin) and a chemical foaming agent were dry-mixed together. The molded mixture is then heat-treated in a three-step process including foaming, debinding and sintering [8]. This process will be discussed in more details in the section 3.2.1.

Titanium, tantalum and their alloys find use in medical devices because of their excellent bio-compatibility. Titanium or tantalum metal foams can be produced using the above discussed methods but the problem of oxide formation can not be ruled out.

Presence of these oxides would make the components unsuitable for medical use. Recent US patent [9] discloses the process in which oxide formation can be prevented with ease by sintering the body in metal hydrides environment. According to this method, polymeric foam is impregnated with a slurry of given metal particles. This slurry is subsequently dried and subjected to pyrolysis and then sintering in metal hydrides environment such as titanium hydride or tantalum hydride. They also have found a method for attaching two metal foam components. In this method, the polymeric foam impregnated with slurry of metal particles is pasted onto the substrate to which attachment is to be done. After sintering, a homogenous attachment of the coating to the substrate is achieved, in particular coating and substrate comprises the same metal [9].

None of the above processes is capable of producing combination of open and closed cell porosity in a controlled way, nor are they capable of creating component directly from CAD design. Nevertheless, a recent US patent [10] has developed a method for these needs, but, their claim is not well supported. They also claim that production of metallic foams is not material specific and it can be used with a wide range of metals, alloys, ceramics and their combination. Materials can be used include, but are not limited to Al, Cu, Mg, Sn, Ti, Zn, Co, Ni, Mo, Nb. Composites and pre-alloyed powders can also be used including stainless steel, Ti64 (Ti-6Al-4V) and many other materials. Similarly wide range of polymer binders can be selected depending on the type of the material used. Below is one of the formulations used to produce foam by this method. Aluminum powder blended with copper powder to produce an Al-4 wt% Cu alloy blend in which PMMA is used as polymer binder [10]. After compressing the blend into feed rods, they were extruded at a temperature in the range of 225 to 250°C. Next the binder burn out

was performed using either flowing nitrogen with 5% hydrogen or followed by furnace cooling. Using this formulation, the cycling binder burnout schedule is carried out which may last for 30 hrs depending on the selected binder [10].

Table 1.1: Percentage mix of constituents used to make Al-4Cu alloy foam [10].

Constituent	Density gm/cm^3	Weight %	Volume %
Aluminum	2.702	95.5	0.542
Copper	8.96	4.5	0.008
PMMA (polymethylmethacrylate)	1.14	-	0.450
Total	-	100	1.00

1.3 Applications of Metal Foams

Cellular metallic materials are finding an increasing range of applications. Metal foams have excellent properties such as, high stiffness-to-mass ratio, high surface area to volume ratio, high permeability, better crash energy and sound absorbing properties. Due to these properties, metal foams find applications in automotive, aerospace, railway, construction industry, machine construction and ship building [2]. There are many criteria which decide its particular application, such as structural or functional. In structural applications, load bearing parts have to be light because otherwise they would be made from conventional massive metals or alloys. Therefore, aluminum, magnesium or titanium foams or other porous metals are preferred for such applications. For medical applications, titanium is usually preferred because of its bio-compatibility. Over a period of time, bones have tendency to grow and porous structure of foam provide them very

good room to grow. This forms excellent mechanical bonding with the foams [9]. Stainless steel or titanium is required for applications where aggressive media are involved or high temperatures occur [10].

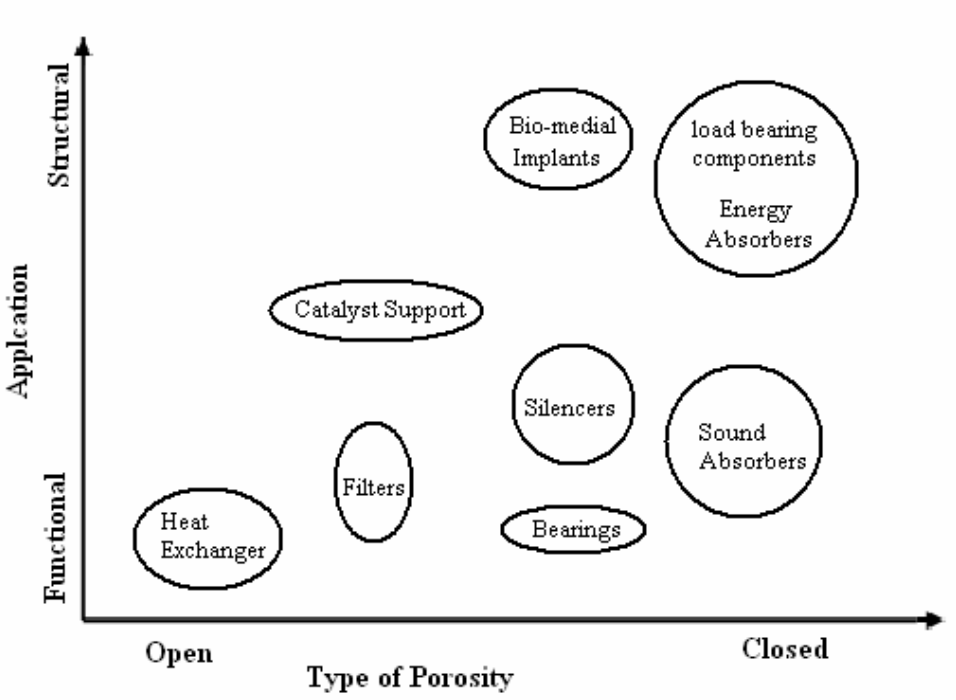

Figure 1.6: The applications of metal foams based on degree of openness [2].

Figure 1.6 explains the applications of metal foams based on the type of porosity. Metal foam can be used as filters, holding back and separating solid particles. Due to its large surface area to volume ratio, highly conductive foams based on copper, aluminum can be used as heat exchangers. An example of such applications; compact heat sinks for cooling of microelectronic devices with a high power dissipation density, such as, computer chips or power electronics. Metal foams can be used as flame arresters; cellular metals with high thermal conductivities of the cell wall material can be used to stop flame

propagation in combustible gases. Metal foams are capable of arresting flames even when they were traveling at velocities up to 550 m/s. Apart from these applications metal foams can be used as silencer, water purifiers or fluid flow controllers [2, 3].

CHAPTER 2

LITERATURE REVIEW

2.1 Transport Properties of Metal foams

Permeability is closely related to the static pressure drop through a porous media. It is defined as the property of a porous medium which characterizes the ease with which a fluid will pass through it under the action of a differential pressure. Permeability is linked with other properties of metal foams such as internal surface area, porosity and pore size distribution [11]. Past studies have confirmed that there is no simple correlation between permeability and other properties [12]. For example, to understand the relation between permeability and porosity, pore diameter and additional parameters must be accounted. Pore diameter is a structural parameter and normally explained by average pore diameter calculated based on statistical pore size distribution. Description of metal foam structure geometrically is a complex task. It is characterized by a variety of geometrical properties such as porosity, specific internal area, pore size distribution and tortuosity. Distinctive property of a natural porous medium is the irregular distribution of the shape and size of its pores. Flow, pressure and other properties, are measured over areas which cross many pores. Such space average quantities, called macroscopic, are the ones of interest in many applications. Unlike the microscopic, at pore scale variables, the macroscopic quantities change in a regular manner through space and with time. Most mechanical and physical properties of metal foam depend on the porosity, the size of the pores and the thickness of the studs of the metal foam and theoretically these are defined by giving the analytical equation of the surface which bounds its pore space.

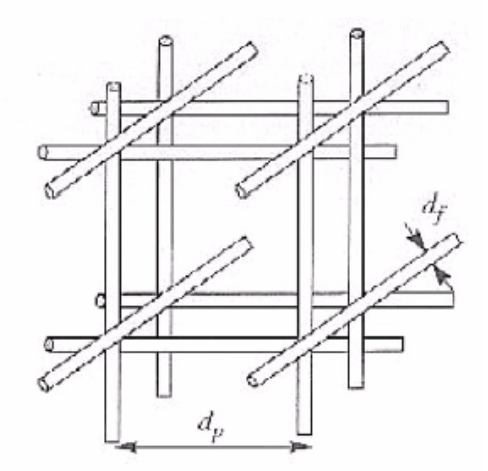

Figure 2.1: Open cell representation of MF [13]

Calmidi [13] proposed an open cell representation to approximate the metal foam structure as shown by Figure 2.1. It is shaped as a cube of unit volume with porosity ε, fibers of diameter d_f and pores of diameter d_p in the x, y and z directions. It has N number of fibers and pores. Hence the solid volume is represented by:

$$3N^2 \times \frac{\pi d_f^{\,2}}{4} \times 1 = (1-\varepsilon) \times 1^3 \tag{2.1}$$

$Since\ \mathrm{N} = \frac{1}{\mathrm{d_p}},$ equation (2.1) can be written as:

$$\frac{d_f}{d_p} = 2\sqrt{\frac{1-\varepsilon}{3\pi}} . \frac{1}{G} \tag{2.2}$$

Where, G is a shape function that takes into account the variation of fiber cross-section with porosity [13]. It is given by $G = 1 - e^{-(1-\varepsilon)/0.04}$. Since open cell representation and true 3-dimensional cells are different, Bhattacharya and Mahajan [14] proposed a relation between d_p and ε in equation 2.2 by characteristic cell size. Cell size is determined by

counting number of cells in a given length of foam and repeating the procedure over different length to get an average value.

Permeability sometimes gets confused with porosity. Porosity is a volume property and represents the content of pores which are not necessarily inter-connected and may not therefore allow passage of a fluid. Generally metal foams with high porosity (>0.9) reduce the pressure drop for the through flow considerably. These foams provide an extended surface area and enhanced heat transfer capabilities [15, 16]. Therefore they are suitable for several applications such as in heat exchangers, filters and flame arresters. Normally porous materials with low porosity are not suitable for such applications where high pressure drop is a major concern. Table 2.1 gives examples of bulk porosity of some common substances.

Table 2.1: Representative values of porosity for various substances [17].

Substance	**Porosity**
Foam Metal	0.98
Fiberglas	0.88-0.93
Wire crimps	0.68-0.73
Soil	0.43-0.54
Sand	0.37-0.50
Cigarette filters	0.17-0.49
Coal	0.02-0.12

2.2 Background on permeability and structural relationship

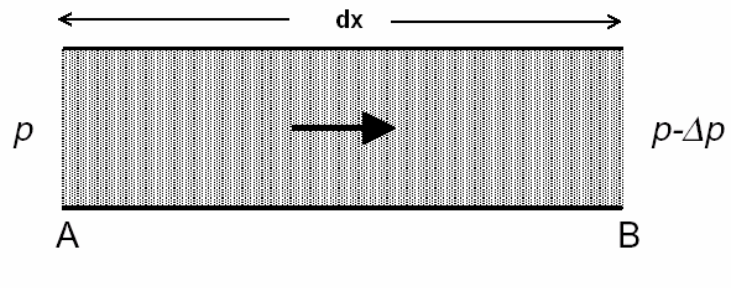

Figure 2.2: Darcy flow through Porous medium [17]

Permeability concept was first put forward by Henry Darcy in 1856 based on lab tests on sand in terms of volumetric flow rate and pressure difference across the sand. Figure 2.2 shows schematic diagram of Darcy's flow. Darcy proposed empirical equation for estimating the volumetric flow rate (Q), which was given by:

$$Q = kA.\frac{dp}{dx} \tag{2.3}$$

Where k = hydraulic conductivity related to porous medium, dx = length of flow path, dp = hydrostatic pressure difference across the specimen and A is the specimen cross-sectional area. Equation 2.3 is presently known to be limited in several aspects. It is valid essentially for incompressible and isothermal slow flow of Newtonian fluid through a relatively long, uniform and isotropic porous medium of low hydraulic conductivity [18]. In most text books Darcy's law is written in the form:

$$\frac{dp}{dx} = \frac{\mu}{K}.V \tag{2.4}$$

Here hydraulic conductivity k of original Darcy's equation is replaced by (K/μ) where K is specific permeability which is defined as independent of fluid properties and μ is fluid dynamic viscosity. It is also known as the Hazen-Darcy equation. It states that the pressure drop per unit length for a flow through a porous medium is proportional to the product of the fluid velocity and the dynamic viscosity [19]. It is clear that Darcy did not consider viscosity effects since his experiments were only with water. Although, viscous and temperature effects were considered important parameters for fluid motion by several scientific works prior to Darcy, for example, Newton in 1687, Navier in 1822, and Poiseuille in 1844 [18]. Hazen [20] first proposed modification to Darcy's law in equation 2.4 to include temperature effects. According to Lage [18], Darcy likely did not compare his work with Poiseuille's work which was based on straight tubes since he worked with sand. Kozeny [21] provided morphological explanation for the fluid viscosity dependency of Darcy's law. He obtained a formulae similar to equation 2.4 by assuming uniform pressure drop and solving Poiseuille's partial differential equations along a discrete capillary length. Dupuit [22], however, made significant contribution in explaining the physics of Darcy's empirical relation mainly based on Prony's [23] previous work since Darcy's original equation 2.3 was based on experimental investigation of the phenomenon of water filtering with limited physical reasoning. Some scientists at that time believed that total resistance to flow is due to two reasons, namely the shear resistance between two neighboring fluid layers and the resistance between the solid and fluid surface. Prony [23] mentioned that the shear resistance should be a polynomial function of the fluid velocity at the solid surface which he verified experimentally and found that quadratic polynomial to be a good fit. Based on this result,

Dupuit [22] proposed a polynomial equation for predicting steady flow through a homogeneous permeable medium based on the reason that the large flow resistance imposed by each small pore being uniformly distributed would induce a uniform fluid velocity.

$$\frac{dp}{dx} = \alpha.V + \beta V^2 \tag{2.5}$$

Even though equation 2.5 was verified experimentally, in several occasions shear resistance cannot be responsible for the quadratic velocity term. The fluid is stagnant at the solid surface and in this event the fact accountable for the quadratic term is the drag force. Drag force imposed to a fluid by any solid surface obstructing the flow path [18]. Using the concept of resistive force to be proportional to the average velocity square as proposed by Newton, equation 2.5, also known as Hazen-Dupuit-Darcy equation, is rewritten as:

$$\frac{dp}{dx} = \frac{\mu}{K}V + \rho.C.V^2 \tag{2.6}$$

Where dx represents the thickness (or length) of porous media, dp is the pressure drop across dx, V is flow velocity, ρ is the medium density, μ is the medium viscosity, K is the permeability and C is the non-Darcian permeability coefficient of the porous media. In equation 2.6, the term ρCV^2 accounts for the inertial effects. Although equation 2.6 is named after Forchheimer in several textbooks and papers, according to Forchheimer [24] himself, he did not develop this equation. Dupuit did instead and credit should be given to him [18]. Lage [18] also mentioned that coefficient C in equation 2.6 should not be used to account for inertia force but for drag force instead, because he assumed that the flow has zero inertia, since it is with constant momentum and inertia is the time rate of

momentum change. A flow through porous medium with constant momentum is a hypothesis and was not supported with an experiment. Lage [18] also stated that Ward's [25] suggestion to replace C in equation 2.6 by ($c/\sqrt{K}$), where c is a constant dimensionless parameter, is not correct since the replacement ignores the effect of solid-form on the flow. Further, this was supported by studies of Beavers *et al.* [26] and Antohe *et al.* [27] that c is not a constant.

Several researchers [18, 25-28] have verified that Darcy's law is valid only for low flow rates where pressure drop is linearly proportional to flow rate. Davis *et al.* [28] have shown that the experimental data sets published by Darcy for higher velocity range ($V > 4\times10^{-3}$) fits quadratic model better than linear model. When velocity increases, the influence of inertia and turbulence becomes more significant and the pressure gradient displays a parabolic trend. At high flow rates, the relation is not linear anymore, instead the pressure drop is found to be higher. This phenomenon is also known as the non-Darcian flow behavior. As the flow velocity increases, the quadratic term becomes more prevalent which must be accounted for an accurate description of the pressure drop [29]. Flow velocity, V, in equations 2.5 and 2.6 can be either Darcian velocity based on the cross-section dimensions of the channel, $V_D = Q/area_{CS}$ or the pore velocity, $V_p = V_D/\varepsilon$ as given by the Dupuit-Forchheimer relation [11, 29]. Pore velocity accounts for the presence of the solid phase in the channel by dividing the Darcian velocity by the volumetric void fraction of the medium. Either V_D or V_p can be used for characterization and derivation of the permeability but one needs to state which velocity is used. In this work, velocity based on cross-section dimension, V_D, will be used.

Permeability of a metal foam is more accurate if determined experimentally [27] since its complex structure is very difficult to model. Several attempts in the past [14, 18, 27, 29] have been made to correlate permeability with other structural parameters of metal foam. Theoretically it is not feasible to determine velocity related to the transition because unknown K has to be measured experimentally. If experimental data is not available, velocity range for Darcian (linear) regime is normally approximated with Reynolds number = 1 criterion that is at the expense of the accuracy. Diedericks and Du Plessis [30] showed that coefficient C is important and becomes significant as the flow velocity increases. The drag force becomes more prevalent and must be considered for an accurate description of the pressure drop. This drag force compensation, C, may vary according to the porosity of the medium and the channel which contains it [31]. Antohe *et al.* [27] reported that K and C are not flow rate dependant but both coefficients are shown to be velocity range dependent. Several researchers adopted Ergun's-like model to explain and fit their experimental results [32-35]. Bhattacharya and Mahajan [14], for instance, mentioned that their experimental results best fit into equation:

$$\frac{dp}{dx} = \frac{\mu}{K}V + \frac{\rho f}{\sqrt{K}}V^2 \tag{2.7}$$

Where, f is the inertial coefficient, also known as Ergun coefficient and K is the permeability, V is the flow velocity. This is widely accepted for steady state unidirectional pressure drop in homogeneous, uniform and isotropic porous medium, fully saturated with Newtonian incompressible fluid. K and f are strongly related to the structure of the medium. Paek *et al.* [33] modeled the inertial coefficient, which depends on tortuosity of porous matrix and flouted model of Du plessis *et al.* [36-37]. They expressed that the Du plessis *et al.* model is valid only for porosities higher than 97%. Du

plessis *et al.* [36-37] modeled metal foam as a rectangular representative unit cell to predict pressure drop using water and glycerol as working fluids. They stated that their model accurately predicts the pressure gradient in flow through metal foam. They reported that inertia coefficient, *f*, reduces with increasing porosity. Recently, Tadrist and Miscevic [32] adopted Hazen-Dupuit-Darcy model in the form of equation 2.5. They demonstrated that the pressure drop with inertial effects is related to the porosity (ε) of the medium and to the average pore diameter (d), using the following equation:

$$\frac{dp}{dx} = A\frac{(1-\varepsilon)^2}{\varepsilon^3 d^2}\mu V + B\frac{(1-\varepsilon)}{\varepsilon^3 d}\rho V^2 \tag{2.8}$$

Where, A and B are constants. Using first term in equation 2.8 to estimate permeability, the following equations can be obtained:

$$K = \frac{d^2\varepsilon^3}{A(1-\varepsilon)^2} \tag{2.9}$$

Comparison between the inertial term in equation 2.5 and 2.8 leads to the following relationship:

$$\beta = \frac{1}{\eta} = B\frac{(1-\varepsilon)}{\varepsilon^3 d} \tag{2.10}$$

However, constants A and B in the above equations have large variation. The major problem, in using the above equations to evaluate the permeability, is defining structural properties of the medium to replace pore diameter (d) reliably. Although the parameter A is clearly quantified for granular media, difficulties arise for metal foam in which it is assumed that the web-like cellular structure made of solid filaments connected in the three dimensions has a particle diameter [34]. Tadrist and Miscevic [32] concluded that there is no clear correlation between porosity, ε, and permeability, K, or inertial

coefficient, *f*, while Paek *et al.* [33] demonstrated that K of a metal foam increases as the cell size increases for fixed porosity. They further added that pressure drop was minimum at the same solid fraction (1- porosity) at different flow velocities is shown in Figure 2.3(a). This indicates that pressure drop depends on cell shape and void fraction. Several researchers [14, 29, 38] reported experimental and theoretical models between porosity and permeability. They reported that permeability increases as porosity increases, Figure 2.3(b) shows an example.

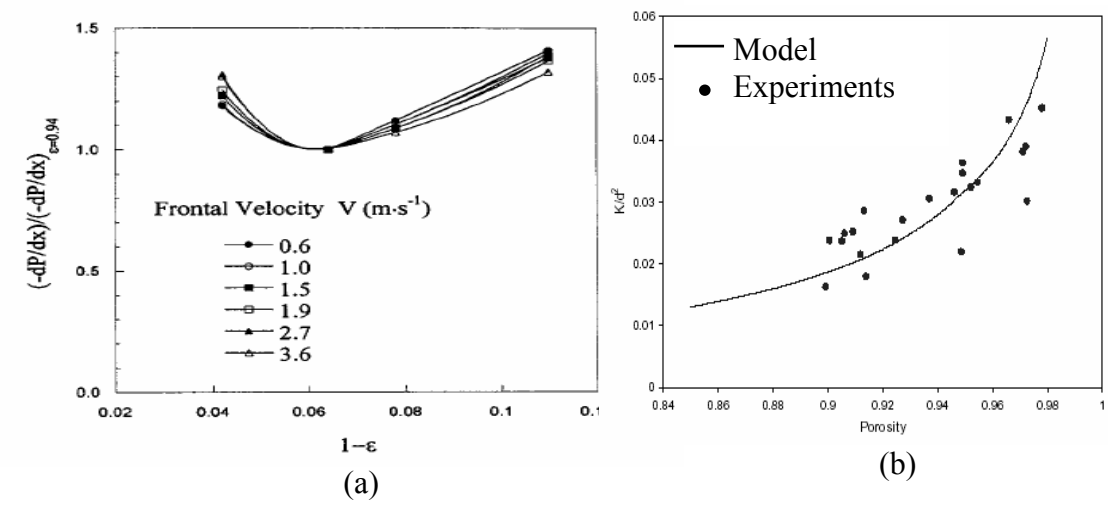

Figure 2.3: (a) Flow velocity and void fraction relationship [33] (b) Permeability and porosity relationship [14]

In open cell foams the main bottlenecks to the flow are the windows that connect one pore to other. Despois and Mortensen [39] used the similarity between these pores and that of spherical sintered particles in a dry powder compact. The permeability of such porous material as a function of the average surface area of the windows between the pores is given by:

$$K = \frac{2(a/\pi)^{3/2}\varepsilon}{\pi d} \tag{2.11}$$

The average window area (equal to the average contact area at the necks between the two particles) is:

$$a = \frac{\pi}{12}\left(\frac{\varepsilon - \varepsilon_0}{1 - \varepsilon_0}\right)d^2 \tag{2.12}$$

Where $\boldsymbol{\varepsilon}_o$ is the initial packing density of the spherical particles (0.64 for the random dense packing of monosized spheres) and ε is the solid density in a particle compact (pore volume fraction in the foam). Despois and Mortensen predicted K of open-cell aluminum foams, using equation (2.11). This prediction was done using Darcian flow regime and therefore, the quadratic term was negligible. But many scientists have correlated the quadratic term to the turbulence of the flow that is inertia. Like Ward [25], Ergun, Fand *et al.* [40] and Boomsma and Poulikakos [29] and the permeability based Reynolds number is:

$$\mathrm{Re}_K = \frac{\rho\sqrt{K}}{\mu}v \tag{2.13}$$

This permeability based Reynolds number has been used to indicate transition from linear behavior in fully developed steady state flow through porous media. According to Boomsma *et al*. [38], the addition of quadratic term has been proven to be applicable for packed beds of spheres for permeability based Reynolds number in the range $80 > \mathrm{Re}_K > 5$. Fand *et al.* [40] confirmed this for randomly packed spheres. While Innocentini *et al.* [41], mentioned that at constant flow rate, without taking into account the temperature effect, an expansion occurs as fluid crosses the medium and therefore entrance and exit velocities can substantially differ from each other. Antohe *et al.* [27] argues that using permeability based Reynolds number to indicate transition from linear behavior as in equation 2.13 is a misconception. Because fully developed steady flow has

zero inertia and hence Reynolds number in the form of equation 2.13 has no meaning. Rather, he suggests using the ratio between form force, D_c, and viscous force, D_μ, as in equation (2.6):

$$\frac{\mathrm{Dc}}{\mathrm{D}\mu} = \frac{\rho.C.V^2}{\frac{\mu}{K}.V} \approx \frac{\rho.C.K}{\mu}.V \tag{2.14}$$

According to Antohe *et al.* [27] the ratio D_c/D_μ reduces scattering of the data observed when permeable media of very different form are used in hydraulic experiments. An analogous proposal has been put forward recently by Du Plessis *et al.* [36], Boomsma and Poulikakos [29] (Figure 2.4) and in another study of permeability of ceramic foam by Innocentini *et al.* [41]. They [29, 36, 41] explained the transition to quadratic behavior, however, they did not agree with Antohe *et al.* [27] on the issue of inertial effects. Du plessis [36] presented experimental results in the form of straight line on a linear-linear graph by rewriting Forchheimer's quadratic equation in the form:

$$-\frac{1}{V}.\frac{dp}{dx} = N + V.M \tag{2.15}$$

Where, N and M are based on morphological parameters of the porous structure and properties of flowing media (μ, ρ). The Darcian region is where N predominates and the Forchheimer's region, where non-linearity is introduced because of large M value. He concluded that Reynolds number at M = N is the Reynolds critical number, which can be found experimentally.

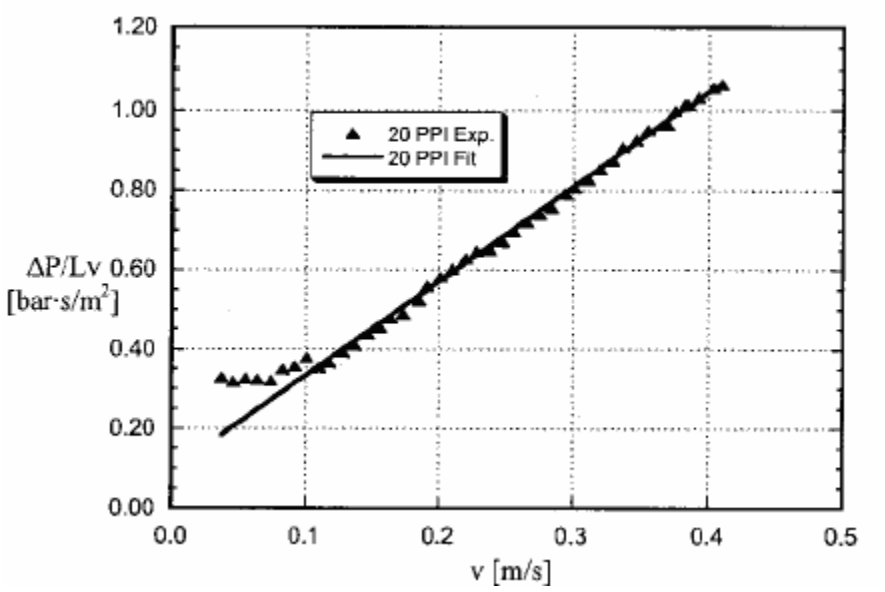

Figure 2.4: ΔP/(Lv) is plotted to show pressure drop deviation from Darcy's law at fluid flow velocities greater than 0.11m/s, the points represents the experimental data [29].

However, very contradicting experimental results of gas flow through ceramic membrane were obtained by Innocentini *et al.* [42]. They concluded that, although pressure drop versus velocity of gas flow through membrane is linear in nature, the quadratic or inertial term can contribute up to 30% of the overall pressure drop. However, it is not clear from their study that the quadratic contribution to the pressure drop is due to inertia. Rather, it is a hypothesis.

The transition from linear regime to quadratic regime occurs at a much lower velocity than that corresponding to Reynolds critical number [18]. According to Lage [18], this may be because of a combined effect of inertia, viscosity, form forces and concepts of macroscopic and microscopic domains. He tried to resolve the confusion by giving example of two different geometries. In the first one, flow through a straight conduit, macroscopic momentum balance for fully developed laminar flow is strictly

between pressure drop and viscous diffusion represented by linear velocity term. In the second case, of disc like body, the balance during transition is mainly between pressure drop and form drag, proportional to the square of fluid velocity. Most porous media are a combination of above two geometries and flow through such medium can depart from linear equation to quadratic equation before transition to turbulence [27, 43]. Inertia forces exist at microscopic or at pore level and form forces are macroscopic in nature, however there is no enough experimental support [27, 43].

2.3 Some analytical permeability calculation models

The attempts to establish empirical correlations between various dynamic properties of porous media all seem to be futile unless certain additional parameters are introduced [11, 41]. Theoretical considerations might be able to attach physical significance to these parameters. The bulk hydrodynamic behavior of porous media can also be obtained from the application of the first principles (i.e. mass and momentum conservation) to the flow of fluids at the pore level. However such an application has been applied to a few simple structures. For complex geometries Navier-Stokes equations should be utilized [44].

2.3.1 Capillary Models

These models are based on fluid flow thorough small diameter complex channels. These models are proposed for obtaining relationships between permeability and porosity and other structural variables for some simple structure such as the matrices made of packed spheres. This is due to the difficulties with large variations in the structures found in natural porous media and other complex manufactured matrices. For flow along straight

tubes of diameter d with cross-sectional distribution of n tubes per unit area, the porosity ε is $(\frac{n\pi d^2}{4})$ [11]. Scheidegger [11] showed, with parallel conduit model that permeability, K = $-\frac{n\pi d^4}{128}$. Since porous medium is much more complex than the parallel-conduit model, this model cannot describe and predict the flow through packed beds. Nevertheless, Scheidegger [11] and later Dullien [44] developed a model for pore structure that consists of capillaries containing segments of variable cross-sections. The experimentally determined variant pore-size distribution is used to assign values for the different rows of capillaries. Dullien [44] model is a combination of parallel and serial arrangement of capillaries. He obtained the permeability of the three-dimensional network using cumulative pressure drop, the Hagen-Poiseuille equation and Darcy law.

2.3.2 Hydraulic Radius Models

The previous model is thus based on series of parallel capillary, however, in reality porous media are different. Hydraulic radius model is a semi-heuristic of flow through solid matrices using the concept of hydraulic radius, Carman-Kozeny theory [45]. The derivation of the Carman-Kozeny relationship (Carman, 1938) is based on the porosity, specific surface area, hydraulic radius, and tortuosity. Since many porous media are composed of random interconnection of the pores, this model was widely accepted in the past. Hydraulic radius is the measure of the ratio of the volume to the surface of the pore space. Kozeny's work recognized the pore structure as having definite details which could be replaced mathematically with a simplified geometry. Hydraulic diameter is defined as:

$$d_h = \frac{4 \times void\ volume}{surface\ area} = \frac{4 \times \varepsilon}{A_o(1-\varepsilon)} \tag{2.16}$$

Where, A_o is specific surface area based on the solid volume, i.e. solid surface area divided by solid volume, (1- ε) is solid volume fraction. Based on this model the permeability is given by:

$$K = \frac{\varepsilon^3}{k_k(1-\varepsilon)^2 \times A_o{}^2} \tag{2.17}$$

Where, k_k is the Kozeny constant, which characterizes the geometry of the porous media. For cylindrical pores, $k_k = 2$. In equation 2.17 the effect of porosity is covered by $(\frac{\varepsilon^3}{(1-\varepsilon)^2})$ and the average particle size is represented by $A_o{}^2$. For uniform spheres packed beds with mean particle diameter d, $k_k = 5,$ and $A_o = 6/d$ thus the empirical equation 2.17 becomes:

$$K = \frac{d^2\varepsilon^3}{180(1-\varepsilon)^2} \tag{2.18}$$

The semi-heuristic Carman-Kozeny model predicts the permeability of packed beds reasonably well but has limited applicability. This model can be used to determine specific surface area and other geometric quantities from permeability measurement provided that Kozeny constants are known. For packed bed of spherical particles with a narrow range of size distribution, Rumpf and Gupte [46] showed that equation 2.17 gives better agreement with their experimental results. They derived the permeability as:

$$K = \frac{d^2\varepsilon^{5.5}}{5.6} \tag{2.19}$$

The experiments were performed with porosity range of 0.35 and 0.67.

2.3.3 Drag Theory Models

In these models, the matrix is considered as a collection of objects. The physical explanation of permeability based on this approach is different. The walls of the pores are treated as obstacles to straight flow of the viscous fluid. The drag of the fluid on each portion of the walls is estimated by solving the Navier-Stokes equation. Then the total resistance to the flow is compared with the Darcyian resistance and then permeability is found [44]. The two specific drag theories are taking obstacles as fibers or as spheres. Based on fiber theory, Happel and Brenner [47] derived permeability for one dimensional flow in cylinder bounded on a solid cylinder diameter d and free cylinder d+δ by a free surface. Figure 2.5 (a) and (b) show cross-sectional view of the arrangement of cylinders for unit cells used for determination of permeability. Permeability is given by:

$$K = \frac{(d+\delta)^2}{16}\left[\ln\frac{d+\delta}{d} - \frac{1}{2}\frac{(d+\delta)^4 - d^4}{(d+\delta)^4 + d^4}\right] \tag{2.20}$$

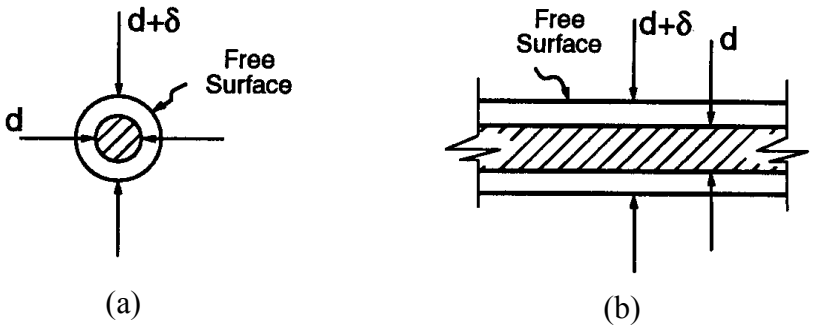

Figure 2.5: Free surface model (a) Flow perpendicular to the cylinder (b) Flow parallel to the cylinder [47]

The Kozeny constant was also derived which was found to be function of porosity. Neale and Nader [48] extended creeping flow model of Brinkman [49] for packing of spheres having diameter d. Brinkman derived permeability as:

$$K = \frac{R^2}{18}\left[3 + \frac{4}{1-\varepsilon} - 3\sqrt{\frac{8}{1-\varepsilon} - 3}\right] \tag{2.21}$$

Since many of the analytical methods assume a cylindrical or spherical shell around the particle, these solutions become less accurate as the porosity decreases and the inter-particle interaction increases. Marchall *et al.* [50] have developed an improvement over these solutions through perturbation expansion of the unit-cell geometry. However, there is a lack of a universal relationship between permeability and porosity. Since it is very difficult to draw analogy between complex structure of the metal foam and capillaries, applicability of the Capillary model is limited. In the Carman-Kozeny theory, the porous medium is assumed to be equivalent to a conduit having a cross section of an extremely complicated shape but constant cross sectional area, on the average. Rumpf and Gupte [46] avoided making any assumptions of that nature. For simple and homogeneous porous structure analogy with geometry could be made with these models, but it should be emphasized that such models neither attempts nor are they able to reflect the complex porous structure. Therefore, in this work Hydraulic radius based model was adopted for simple and homogenous structures. For intricate structures, effort is made to identify the structure parameters that are responsible for different pressure drop behaviors.

2.4 Objectives

For many applications, the permeability is an important parameter to characterize and optimize. The parameters affecting the permeability of metal foams identified in the literature as porosity, pore diameter and tortuosity. The structures of metal foam are very intricate and irregular, which nearly rules out the possibility of analytical approaches. Most of the studies have therefore been directed towards experimental measurements. The aim of the present work is to categorize various structural parameters responsible for the observed pressure drop across the metal foam, especially to understand the impact of simple and intricate microstructures. The Recemat and IMI metal foam samples are made from metallization of polyurethane foam by electro-discharging and powder metallurgy approach, respectively. The former has well distributed and uniform pore structure, while the latter has irregularity of the cell structure. The aim of the present work is also to build the equipment which accurately measures, the pressure drop across such foams. Experiments are conducted at higher velocities of flowing media in order to understand the impact of inertia.

CHAPTER 3

EXPERIMENTAL INVESTIGATION AND SAMPLE PREPARATION

3.1 Experimental equipment and procedure

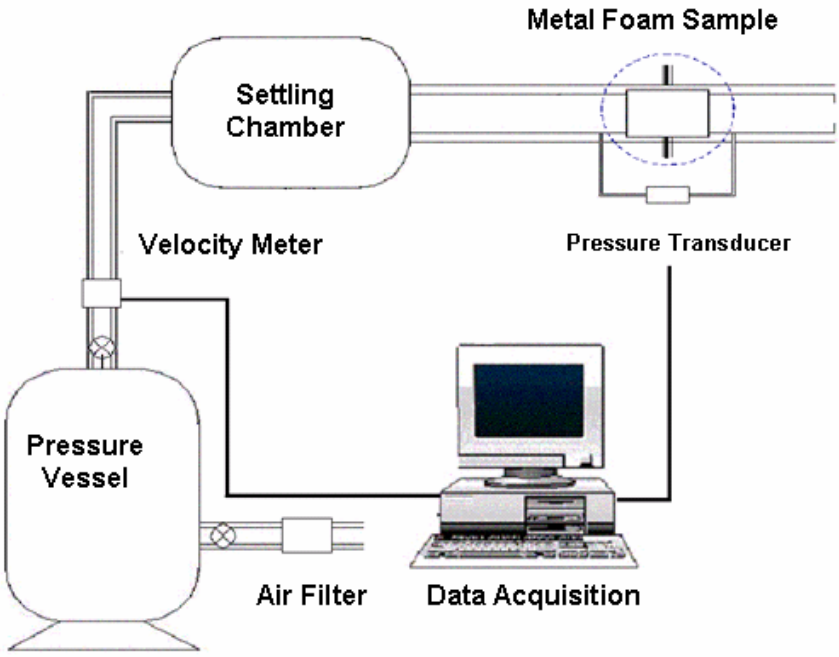

Figure 3.1: Experimental Setup

The experiment on the MF samples was conducted using the instrument shown in Figure 3.1. It consists of a middle flange assembly, a pressure transducer, a velocity meter, a pressure vessel and a settling chamber. Following the experimental set-up by Paek *et al.* [33] and ISO4022-1987-10-01 standards, it was designed and built to obtain accurate determination of the flow and pressure drop across the sample. This set-up was designed to use compressed air as flowing media. Compressed air was allowed to fill the pressure

vessel at particular pressure value. The pressure was controlled by manual pressure control-valve. Air filter was employed in line prior to pressure vessel, so that any impurities or foreign particles could be cleaned. Air was then allowed to pass through settling chamber by means of 2 inch steel pipe. Settling chamber avoids any possible turbulence in the flow. Finally air from settling chamber was permitted to pass through metal foam assembly.

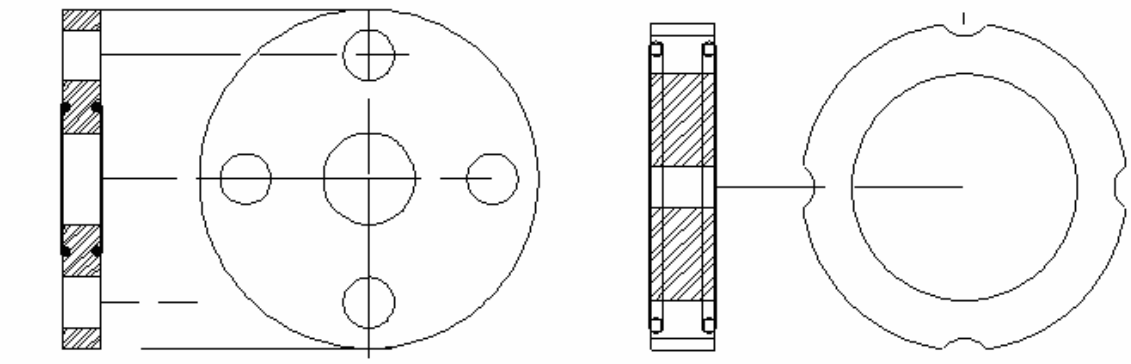

(a) *(b)*

Figure 3.2(a): Mid-flange for IMIMF samples, (b): Mid-flange for RMF samples

Metal foam sample is securely assembled to a middle flange as illustrated in Figure 3.2 (a) and (b). The mid-flange assembly was placed in a 1 inch steel pipe and was held securely by two end flanges as shown in Figure 3.3. IMIMF samples were insulated to prevent air-bypass and to fit well with the mid-flange. Teflon tape was used to insulate the samples. RMF samples were quite tight on the middle flange so insulation was not necessary. Light pressure was used to push the samples in mid-flange assembly. This was done carefully to avoid any shearing or permanent deformation of the sample. Visual inspections did not reveal any physical changes in the samples. For IMI samples mid-flanges with different thicknesses (5, 10, 15mm) were manufactured to accommodate

samples with various thicknesses. Pressure taps were drilled on the pipe as close to the sample as possible and one way valves were used to prevent air flow from the hole. The pressure at downstream was atmospheric, which was confirmed by measurement. Thus

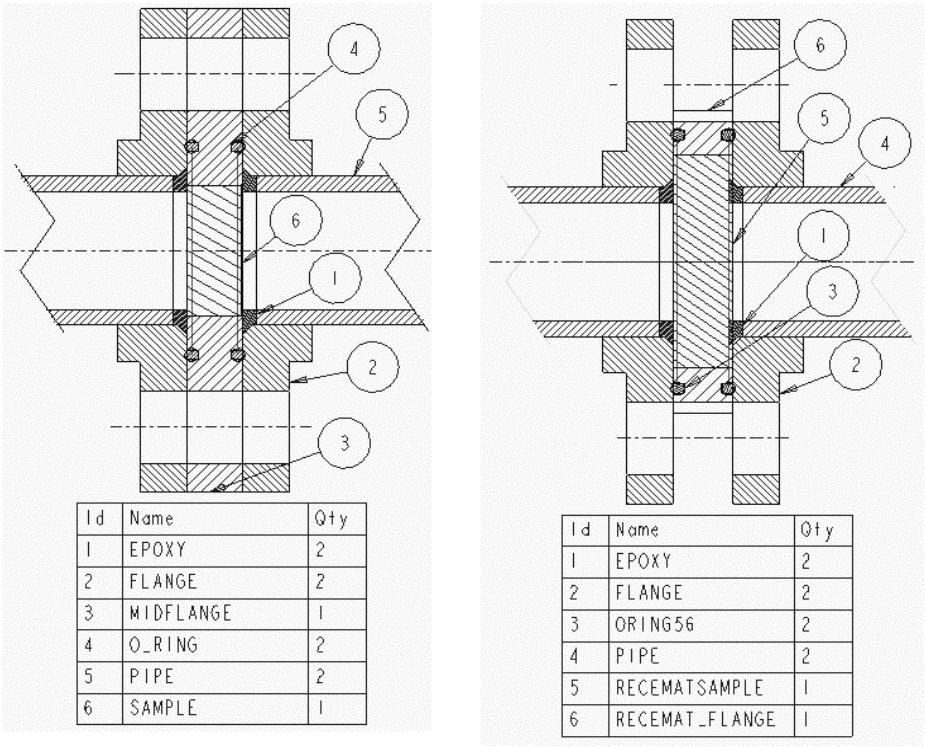

Figure 3.3: Flange Assembly (a) IMIMF (b) RMF

only upstream pressure was measured using OMEGA pressure transducer for gauge pressure range 0-25 gauge (psi) with an accuracy of ±0.1% full scale. Flow velocity was measured using OMEGA velocity meter for the flow velocity range of 0-1000 standard ft/min with ±1% full scale accuracy. The acquisition of signals from the velocity meter and pressure transducer was gained by data acquisition device manufactured by OMEGA which was subsequently connected to the computer. InstaCal software, provided by OMEGA was installed to configure data acquisition device. Lab-view software was used to program the required set-up, read the sensors and finally to write the data into the

output file. With this configuration, the pressure and flow data were viewed and recorded to the computer hard drive in real time. During a typical experimental run, the set-up was first tested for any leaks. Airflow rate through the metal foam was set at desired value using a valve. A series of experiments were performed. To minimize the error for each experiment, 100 data sets were collected and the average was used to plot the graphs. IMIMF and RMF were made from nickel and nickel-chromium, respectively. Disc diameter of Recemat metal foams were 47 mm whereas IMI metal foams were 29mm. Recemat metal foams were made bigger by the manufacturer in order to match the field installation conditions, since it is used in flame arrester application to withstand high pressure (300psi). However the effective area in both types of metal foams is the same.

3.2 Sample preparation

3.2.1 IMI metal foams

Open cell IMIMF samples were made by powder metallurgy approach. A metal powder, a solid polymer binder (i.e. resin) and a foaming agent were mixed in a known proportion. The mixture was molded then heat-treated in a three-step thermal treatment to produce MF. Nickel MF samples were produced for testing. For all the samples, the main manufacturing conditions, sintering temperature ($900^{o}C$) and composition (Ni Powder 3-7 μm, Phenolic Resin and P-toluene sulfonyl hydrazine) were the same. A more detailed process description is given in [8, 51]. Figures 3.4 and 3.5 illustrate the steps followed. During sintering, solid-state diffusion results in metallurgical contacts between the

metallic particles which improve the mechanical properties. Mechanical properties and surface area of metal foam are function of sintering temperature.

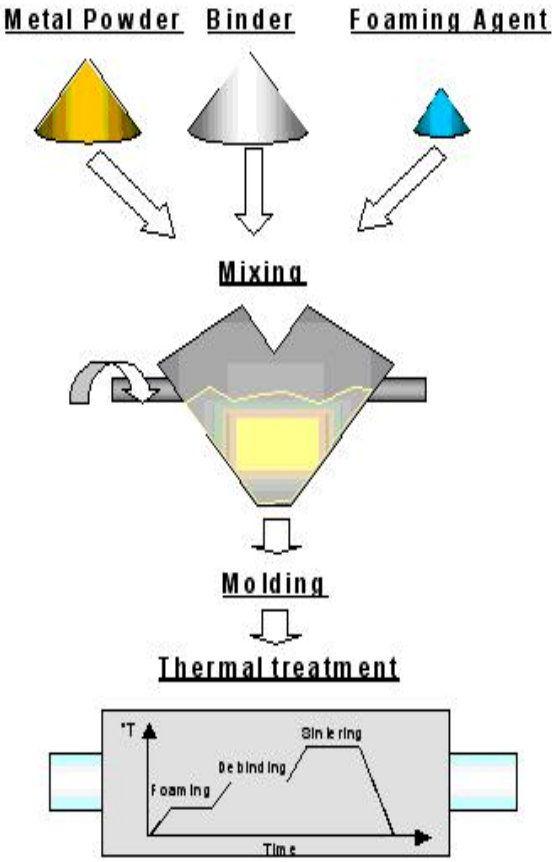

Figure 3.4: Producing IMI metal foams by using powder metallurgy approach [51]

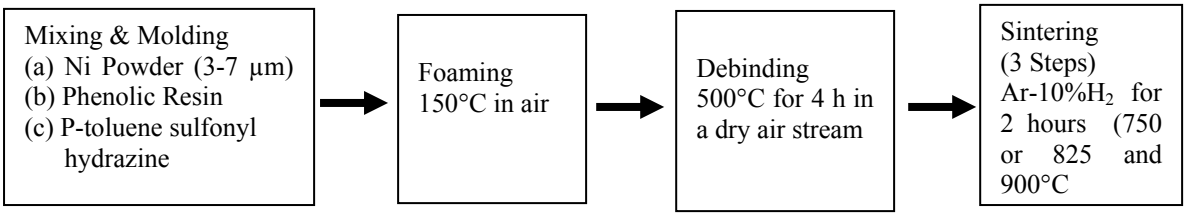

Figure 3.5: Illustration of IMI Metal Foam Production Steps

The higher sintering temperature improves mechanical properties at the expense of surface area [8]. Figure 3.6 shows a typical microstructure of an IMI metal foam. Table 3.1 lists the different IMIMF samples that were studied in this work.

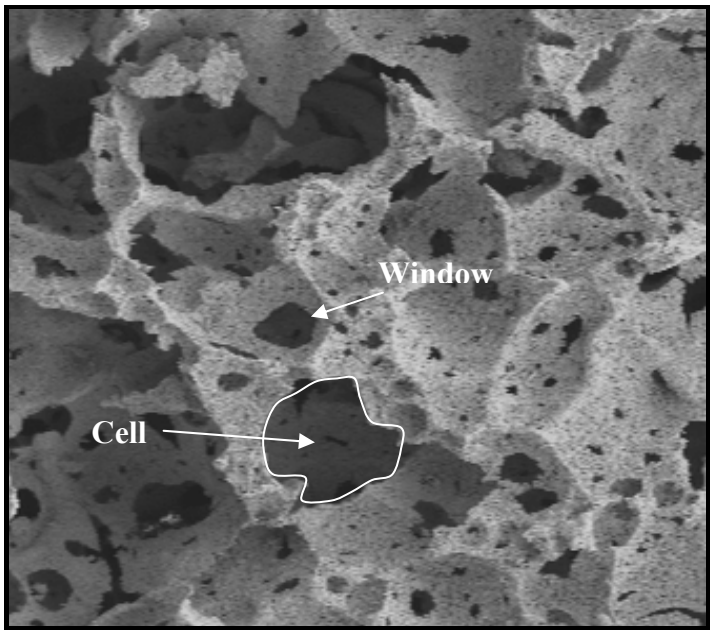

Figure 3.6: Microstructure of Metal Foam produced at the IMI, sample Ni-70 1A4

Table 3.1: IMI metal foam samples

Sample	Thickness (dx), mm
Ni7005-1A3	11.85
Ni7005-1A4	11.40
Ni7005-1A5	11.40
Ni6005-1A2	8.38
Ni6005-1A3	8.96
Ni6005-1A4	8.27

3.2.2 Porosity measurements of the IMI metal foams

Porosity of the metal foam given by the equation:

$$\varepsilon = 1 - \frac{V_{solid}}{V_{foam}} \tag{3.1}$$

Where, V_{solid} is solid phase volume and V_{foam} is total foam volume.

Volume of the foam in equation 3.1 can be measured easily by measuring dimensions of the samples, but measuring the volume of the pores is more complicated. This can be performed by means of gas pycnometer to measure density. The equipment used for the measurements was Micromeritics 1305. This equipment consists of two separated closed chambers of known volume. The material is inserted in one of the chambers, and the other is pressurized to a selected pressure. Then, a valve between the two chambers is opened and the pressure is allowed to equilibrate in the whole system. During filling, the gas flows in all the pores of the sample. The volume, found by gas law, is compared to the mass of the sample to obtain the density. These measurements were carried out at IMI, Boucherville, Canada. Five readings of each sample were taken and then averaged. Table 3.2 shows a comparison between the measured and calculated values. Density of the Nickel (Ni) powder is measured to be $8.82^{\pm 0.02}$ gm/cm^3. It is clear that the porosity for all Ni60 was found to be in the range of 91 to 93%, while for Ni70 samples, it is in the range 89.88 to 91%. Standard deviation for Ni60-1A2 and Ni60-1A3 is high compared to other samples.

Table 3.2-I: Porosity measurements for IMI samples.

Sample	Density, gm/ cm^3	Std. Deviation	Apparent Volume, cm^3	Wt. gm	Volume of solid, cm^3	
					Measured	Calculated
Ni60-1A2	6.91	0.178	5.53	2.78	0.403	0.315
Ni60-1A3	6.15	0.362	5.45	2.94	0.480	0.334
Ni60-1A4	6.25	0.100	5.12	2.47	0.395	0.280
Ni70-1A3	7.28	0.083	5.28	3.89	0.535	0.441
Ni70-1A4	7.20	0.063	5.42	3.71	0.516	0.421
Ni70-1A5	7.26	0.034	6.08	4.17	0.574	0.472

Table 3.2-II: Porosity measurements for IMI samples

Sample	Porosity , %			closed voids %
	Measured	Standard Error	Calculated	
Ni60-1A2	92.72	0.08	94.30	1.57
Ni60-1A3	91.19	0.22	93.87	2.68
Ni60-1A4	92.28	0.06	94.53	2.24
Ni70-1A3	89.88	0.05	91.65	1.76
Ni70-1A4	90.47	0.04	92.22	1.75
Ni70-1A5	90.56	0.02	92.22	1.67

3.2.3 Recemat metal foams (RMF)

RMF is a commercially available MF for several decades. It is an open cell polyurethane foam metallized using EDT (Electro-discharge technique). This process has superior control on the cell size because preform structure determines the foam microstructure.

The detailed process description is given in [2, 52]. Figure 3.7 shows a typical RMF microstructure. Nickel-chromium (NC) and nickel-chromium extra strong (NCX) metal foams with 5 mm, 10 mm and 13 mm thick RMF samples were tested. These samples are listed in Table 3.3. Samples are coded by material and grade number. Each grade is available in standard thickness and size.

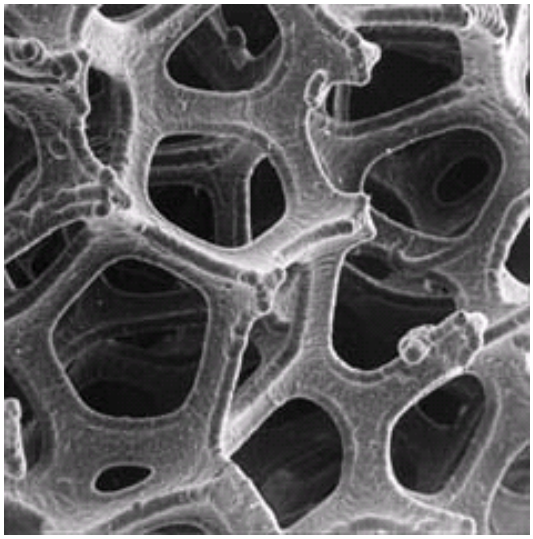

Figure 3.7: A typical RMF microstructure [52]

Table 3.3: RMF Samples

Thickness →	**5mm**	**10mm**	**13mm**
Samples Grades	*	NCX 1116	NCX 1116
	*	NCX 1723	*
	NC 2733	NC 2733	*
	*	NCX 2733	*
	NC 3743	*	*
	NC 4753	*	*
* Indicates that samples are not produced.			

Table 3.4 shows some of the RMF structural properties. The grade relates to the range of pores which is the approximate number of pores per linear inch (25.4 mm). The surface area to volume is also tabulated. Data in Table 3.4 are provided by the Recemat International, Netherlands based MF manufacturer.

Table 3.4: RMF structural properties [52]

Grade #	**Range of pores (pores / inch)**	**Average Pore diameter (mm)**	**Specific surface area (m^2/m^3)**
1116	11 ... 16	1.4	1000
1723	17 ... 23	0.9	1700
2733	27 ... 33	0.6	2500
3743	37 ... 43	0.5	3700
4753	47 ... 53	0.4	5600

3.2.4 Porosity measurements of the Recemat metal foam

The RMF average porosity was estimated using equation 3.1. Volume of foam is based on the sample dimensions. The solid volume of the MF is calculated by weighing each sample and dividing it by the average measured density ($5.16^{\pm 0.20}$ gm/cm^3). The results of porosity measurement are listed in Table 3.5. Average density was measured using the ASTM-792-98 standard. The total foam volume is measured directly. The actual sample thickness was also measured and tabulated along with estimated porosity. These porosity data were then averaged from three replicas of the same grade and the averaged values were used in further calculations.

Table 3.5: Volumetric Porosity of Recemat Metal Foam

	Sample #	**Thickness (dx)(mm)**	**Weight (gm)**	**V_{foam} (mm^3)**	**V_{solid} (mm^3)**	**ε**
NC1116-10, d= 1.4mm, dx= 10mm	1	10.01	8.5	17 377	1 647	0.91
	2	10.00	8.7	17 356	1 686	0.90
	3	10.40	11.0	18 051	2 131	0.88
NC1116-13, d=1.4mm, dx=13mm	1	13.23	15.4	22 966	2 984	0.87
	2	13.27	13.1	23 035	2 538	0.89
	3	13.24	12.9	22 980	2 500	0.89
NCX1723-10, d=0.9mm, dx=10 mm Extra Strong	1	10.17	9.4	17 648	1 821	0.90
	2	10.40	11.1	18 051	2 151	0.88
	3	10.23	10.3	17 759	1 996	0.89
NC2733-5, d=0.6mm, dx=5mm	1	4.87	4.6	8 456	891	0.89
	2	5.10	4.7	8 859	910	0.90
	3	4.90	4.4	8 512	852	0.90
NC2733-10, d=0.6mm, dx=10mm	1	10.00	10.0	17 363	1 937	0.89
	2	10.20	9.4	17 704	1 821	0.90
	3	10.20	9.9	17 704	1 918	0.89
NCX2733-10, d=0.6mm, dx=10 mm Extra Strong	1	10.34	14.0	17 953	2 713	0.85
	2	10.40	14.7	18 051	2 848	0.84
	3	10.23	14.7	17 752	2 848	0.84
NC3743-5, d=0.5mm, dx= 5mm	1	5.16	7.8	8 956	1 511	0.83
	2	5.20	7.7	9 025	1 492	0.84
	3	5.10	7.6	8 852	1 472	0.83
NC4753-5, d=0.4mm, dx=5mm	1	5.30	6.0	9 206	1 162	0.87
	2	5.31	6.3	9 220	1 220	0.87
	3	5.30	7.1	9 206	1 375	0.85

3.2.5 Scanning Electro-Microscopy

Microstructure of the IMIMF was studied by SEM analysis. SEM was performed at IMI, Boucherville, Canada by the Jeol-JSM-6100 scanning electron microscope, while SEM images were analyzed at Concordia University using the image analysis software 'analySIS' version 3.2. SEM pictures of the sample were taken at different zones. Five such zones were randomly selected; however, all zones were well separated from each other.

The JSM-6100 is equipped with a digital image processor. It has a large specimen chamber that allows observation of the entire surface of a specimen up to 150 mm and a tilt of -5 to 90^{o} is possible. Samples with poor electrical conductivity are either coated with an electrically conductive coating or studied at low voltages (which does not give backscatter or X-ray information). Electrically conductive coating takes time but improves images. The operating accelerating voltages is 5-30 kV and resolution: 4.0 nm at 30 kV and 8 mm working distance. Magnifications were selected so that appropriate topographic details could be captured. Images captured were taken at two magnifications: for cell windows at x75 and for cells at x25.

CHAPTER 4

RESULTS AND DISCUSSION

4.1 Results

The pressure drop data for MF was normalized per unit length using actual sample thickness (dx). The permeability and non-Darcian permeability co-efficient were determined for each sample using the entire velocity range of 0 m/s to 20 m/s by a curve fitting procedure. During the experiment, the flow is fully developed. Equation 2.5 is used for curve fitting which is widely accepted model and used by several researchers [14, 33, 34, 38]. A least squares fit was performed to determine the values of α and β in equation 2.5. Correlation coefficient squared (R^2) value indicates the proportion of variation in pressure drop relative to flow velocity. In most cases R^2 is greater than 98%, except for two samples (NC2733-10 and NC3743-5) where R^2 is around 97%. This indicates that the 2nd order quadratic relationship is valid for most of the cases, unlike Antohe *et al.* [27] who proposed cubic extension of the equation. Pressure drop can be predicted in the tested velocity range with an error less than 2%. Comparing equations 2.5 and 2.6, values of K and C were calculated as:

$$K = \frac{\mu}{\alpha}, \quad C = \frac{\beta}{\rho} \tag{4.1}$$

Dynamic viscosity and density of air are taken as 1.85 $\times 10^{-5}$ pa.s and 1.225 kg/m^3, respectively. Several tests were performed on the same sample to check for the repeatability and hysteresis. Since the flow is steady-state, unidirectional pressure drop through the medium, no hysteresis was noticed and experiments with the same samples

were repeatable. This can be seen in Figure 4.1 which presents one of the repeatability tests performed on Ni60-1A4 sample. This figure shows that data points from two different tests are overlapping. Figure 4.2 shows an example of two RMF samples with the same pore diameter (0.6 mm) and two different thicknesses (5 and 10 mm). Thickness, dx, represents the average value of 3 samples of 0.6 mm pore diameter.

Pressure drop is a function of pore diameter. As pore size of the metal foam decreases, the surface area to volume ratio increases creating additional flow resistance. This leads to an increase in the pressure drop. The repeatability of the measurements is achieved by performing the experiment on 3 replicas for each grade. This provides information on K and C variation, within the samples with same grade and thickness. Pressure drop results show that the flow through open cell metal foams deviates from Darcy's law and the pressure drop across the foam is a quadratic function of the flow velocity as suggested by many researchers.

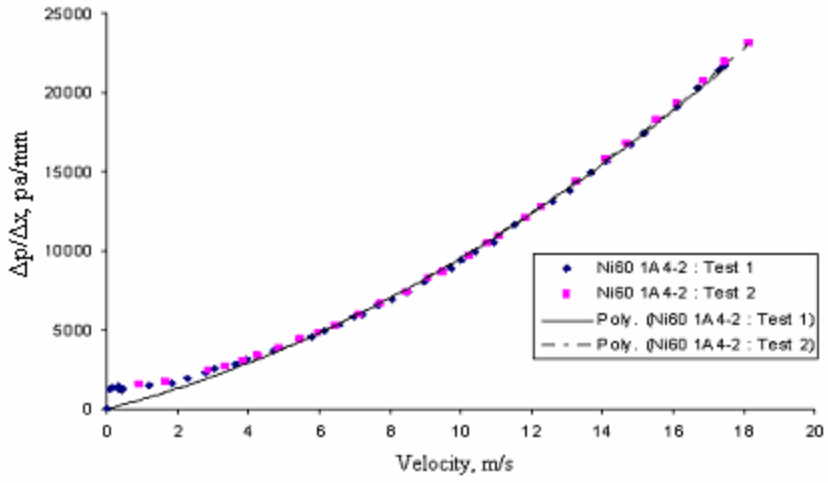

Figure 4.1: Repeatability test showing no variation between the two test.

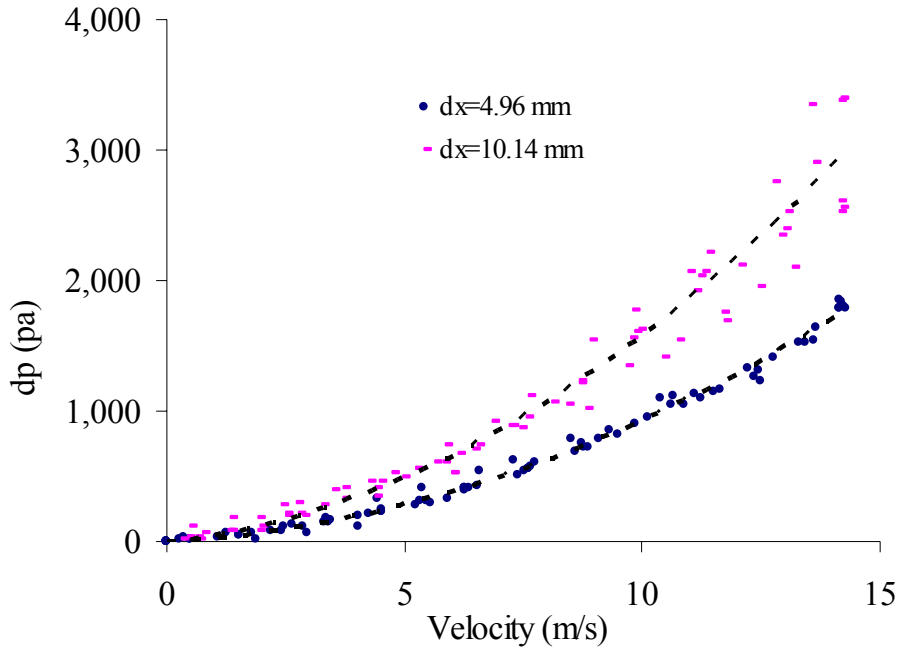

Figure 4.2 : Thickness (dx) effect on pressure drop on RMF for d=0.6 mm (not normalized)

4.1.1 Recemat metal foams results

For various Recemat metal foam samples, pressure drop was measured at different velocities as can be seen in Figures 4.3 and 4.4. These results are obtained by averaging the values of the three replicas of each grade. It can be seen that as the pore size increases pressure drop decreases.

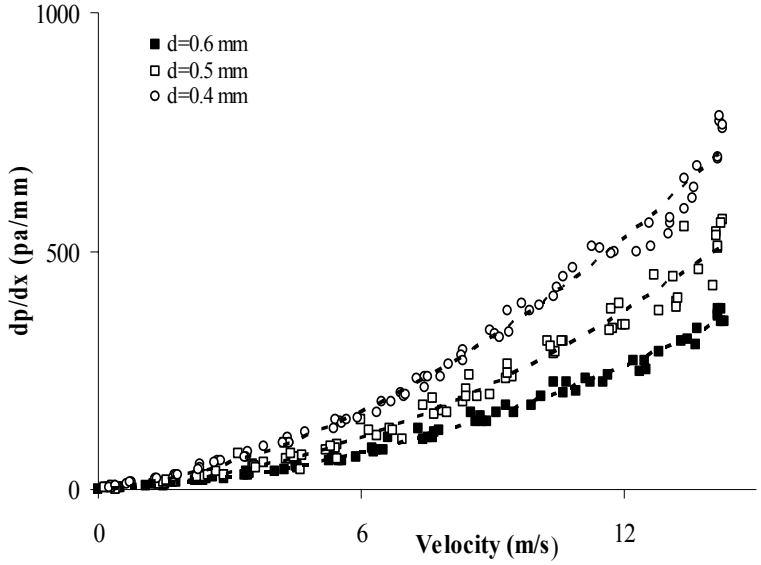

Figure 4.3: Pressure drop per unit length versus velocity for 5 mm thick RMF

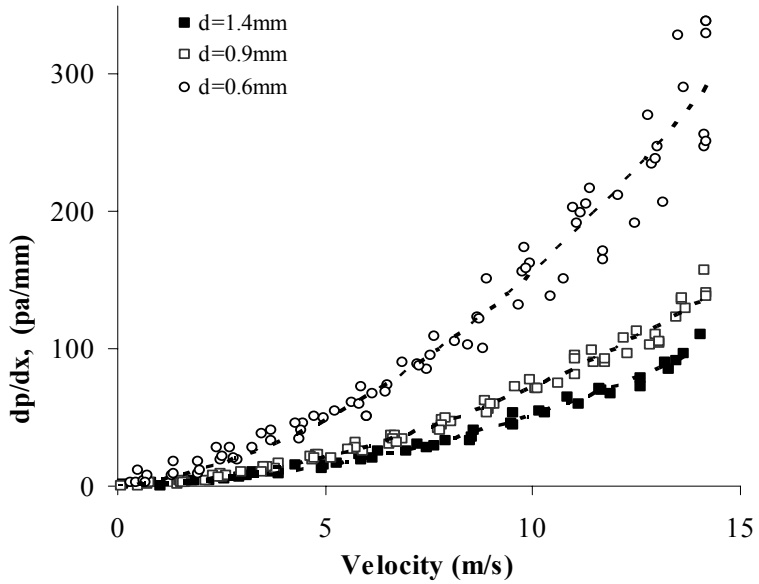

Figure 4.4: Pressure drop per unit length versus velocity for 10 mm thick RMF

Table 4.1 shows that, for the largest pore diameter RMF (d = 1.4 mm), K value is highest whereas C is lowest. For the smallest pore RMF (d = 0.4 mm), however, K is lowest whereas C is highest. This indicates that K and C are highly correlated with pore diameter for this foam.

Table 4.1: Quadratic curve coefficients (α and β), K (m^2) and C ($m^{-2}\ s^2$) for RMF

Description (d, dx)	$\alpha = \mu / K$	$\beta = \rho.C$	R^2 %	K ($\times 10^{-9}$)	C ($\times 10^{3}$)
(1.4 mm, 10 mm)	0.6692	0.4541	99.0	27.64	0.37
Extra Strong (0.9 mm, 10 mm)	1.20	0.5997	98.87	15.39	0.49
(0.6 mm, 10 mm)	3.75	1.1802	96.27	4.93	0.96
(0.6 mm, 5 mm)	3.93	1.47	99.25	4.70	1.21
(0.5 mm, 5 mm)	5.49	2.14	97.98	3.37	1.75
(0.4 mm, 5 mm)	10.52	2.77	99.07	1.76	2.26

Figure 4.5 and 4.6 illustrate K and C values, recpectively, for RMF at different pore diameters. For d = 0.6 mm, average value was calculated from three sets of each thickness. Average values of K and C are listed in Table 4.1

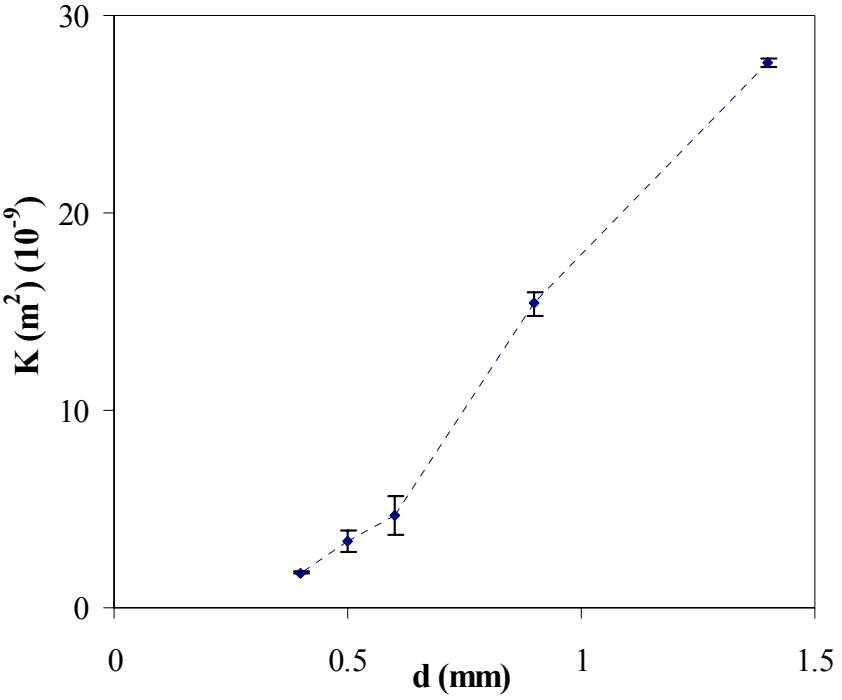

Figure 4.5: Permeability for different pore diameter RMF

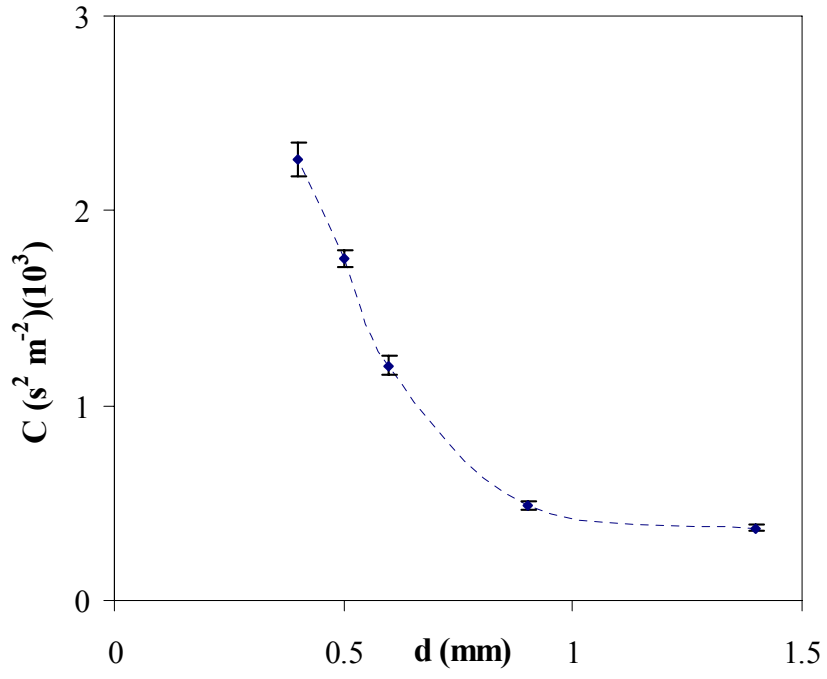

Figure 4.6: Non-Darcian Permeability for different pore diameter RMF

The effect of thickness on the permeability of metal foam was also observed. For the same pore diameter (d = 0.6 mm) MF, 5 mm and 10 mm thick samples showed only slightly different values of K (4.70 and 4.93). This indicates that the increasing thickness of the MF has marginal effect on K and C. This is probably due to uniform morphology of the MF over the length. This could be seen in Figure 4.7, which presents the unit pressure drop for two different thicknesses but with the same pore diameter d = 0.6 mm. Hence, this small variation in the values of K and C is a result of similar pressure drop characteristics of the two samples.

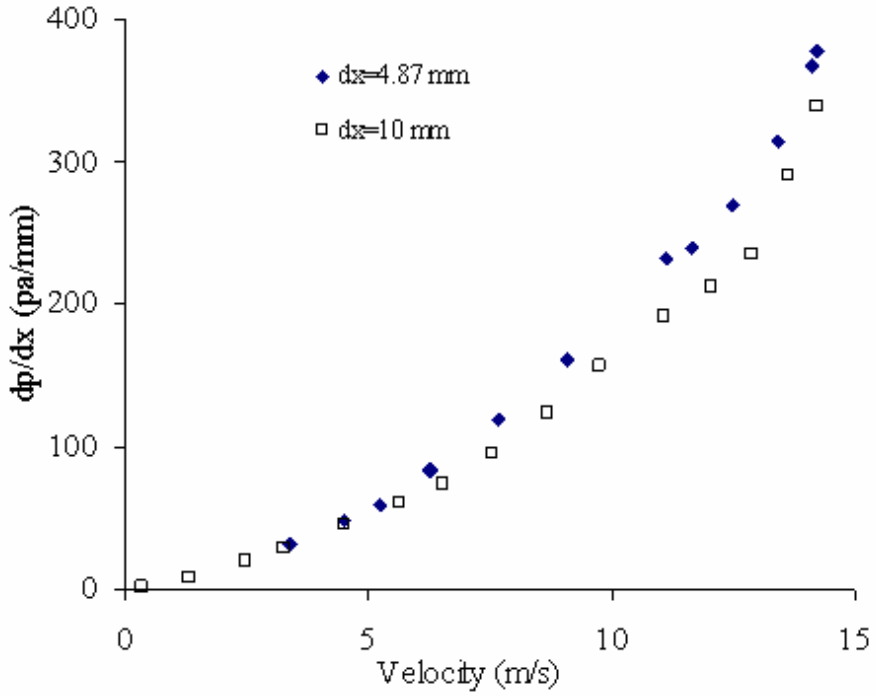

Figure 4.7: Unit pressure drop versus velocity for 5 mm and 10 mm thickness at 0.6 mm pore diameter

For large pore diameter samples (d = 1.4 mm, dx = 13 mm), coefficient α in equation 2.5 was negative. Setting α zero, K becomes infinite, the predicted data was still in good agreement with experimental pressure drop. This indicates that pressure drop in large pore RMF was mainly due to drag force and/or inertial effect of the flowing fluid. Fitting the data in 3rd order curve slightly improves R^2 value, but 2nd order curve was selected for calculating the K and C because it is more scientifically based. Figures 4.8 and 4.9 illustrate K and C at different velocity ranges for 5 mm thick RMF.

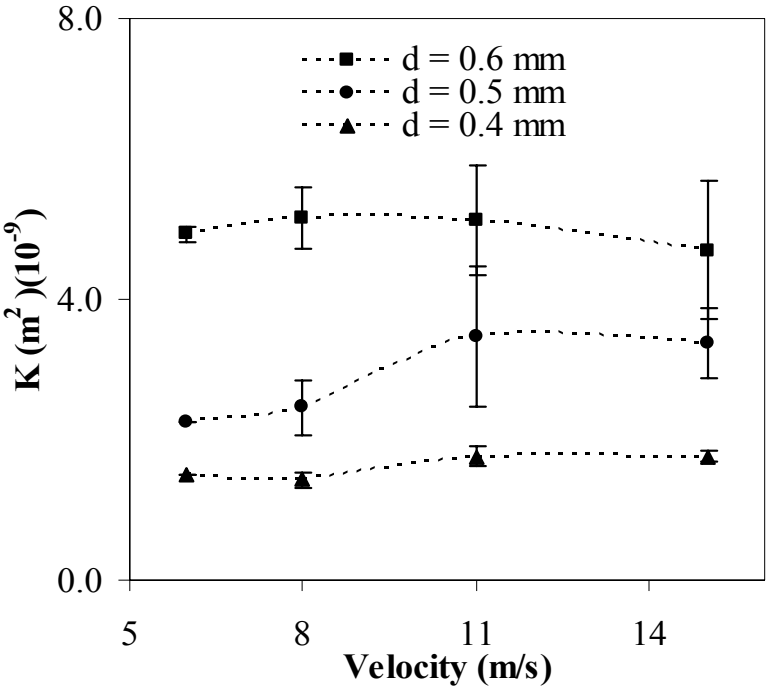

Figure 4.8: Permeability at different velocity range for 5 mm thick RMF

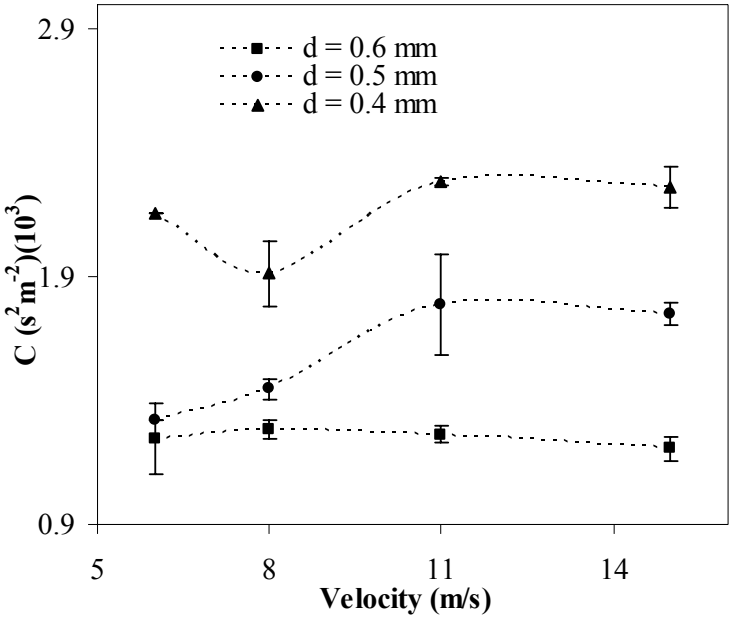

Figure 4.9: Form coefficient at different velocity range for 5 mm thick RMF

For the whole velocity range (0 - 15 m/s), K is lowest whereas C is highest for d = 0.4 mm. This indicates that in the smaller pore foam, the major pressure drop contributions are from quadratic term. For the whole velocity range (0 - 15 m/s), velocity had no significant effect on the K. However, standard error in the measurements of K was high at higher velocity range (8 - 15 m/s). This may be due to variation in the morphology among three replicas of same grade samples. The standard error among measurements of C was comparatively lower. Figures 4.10 and 4.11 represent the permeability and non-Darcian permeability (K and C) for different velocity ranges.

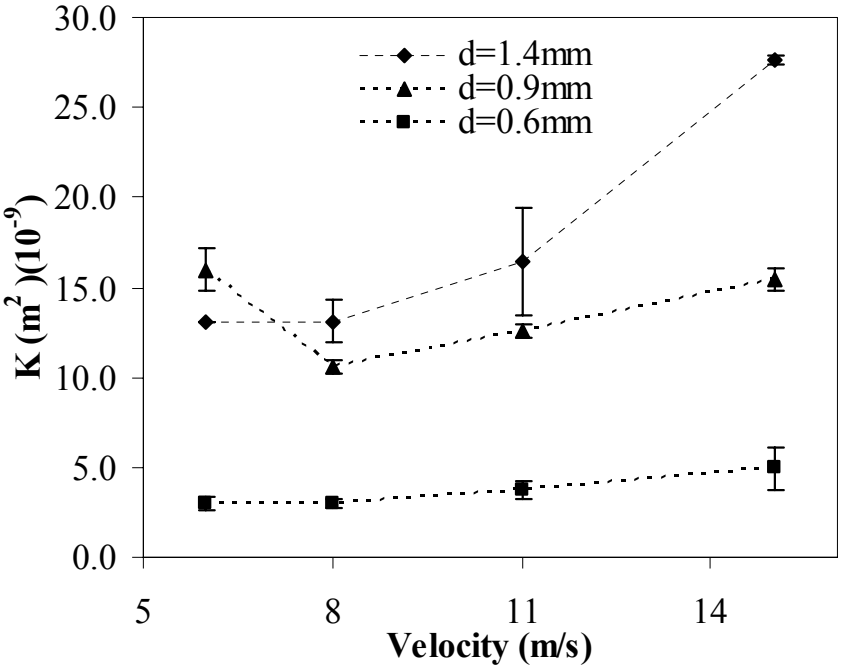

Figure 4.10: Permeability at different velocity range for various 10 mm thick RMF

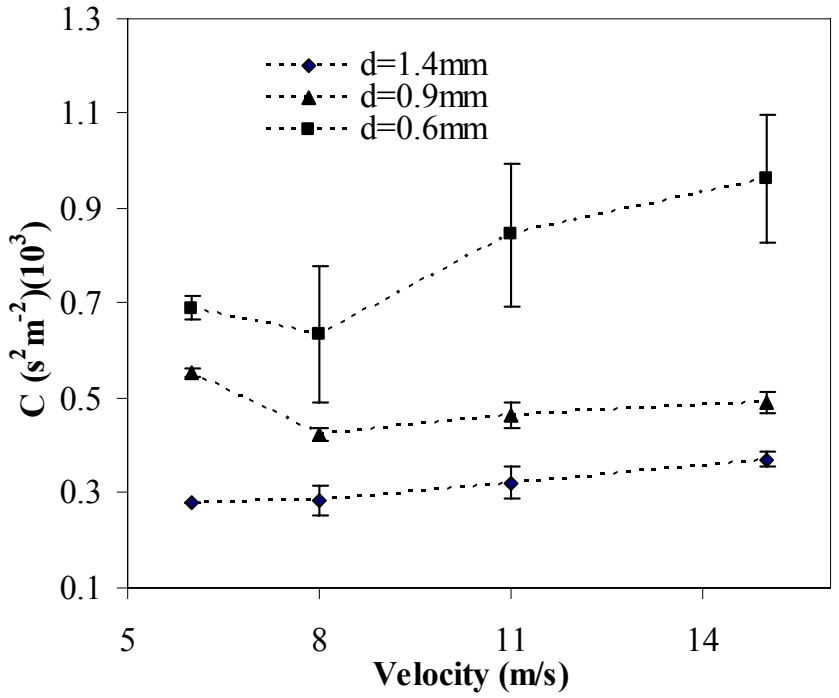

Figure 4.11: Form coefficient at different velocity range for various 10 mm thick RMF

For larger pore diameter (d = 1.4 mm), permeability varys significantly over higher velocity range, as can be seen in Figure 4.10. K and C at different velocity ranges for RMF samples were listed in Table 4.2. Figures 4.12 and 4.13 show the K and C for different porosities. The average porosity of the samples of pore size 1.4 to 0.4 mm was 0.90, 0.89, 0.90, 0.83 and 0.86. Apparently, K shows no special trend with porosity. However, even if the data points are seen as scattered from a trend line, the increasing relationship could be established for K, vice versa for C. Many researchers in the past tried to explain the permeability relationship with the porosity, which shall be discussed later.

Table 4.2: K $m^2(\times 10^{-9})$ and C (s^2m^{-2}) $(\times 10^3)$ at different velocity range

Sample description (d, dx)	**Permeability Factor**	**<6**	**<8**	**<11**	**<15**
Pore diameter - 1.4 mm, Thickness - 10 mm	K	13.09	13.11	16.43	27.64
	C	0.28	0.29	0.32	0.37
Pore diameter - 0.9 mm, Thickness - 10 mm (Extra Strong)	K	15.96	10.59	12.57	15.39
	C	0.56	0.42	0.46	0.49
Pore diameter - 0.6 mm, Thickness - 10 mm	K	3.02	2.98	3.76	4.93
	C	0.69	0.63	0.84	0.96
Pore diameter - 0.6 mm, Thickness - 5 mm	K	4.92	5.17	5.12	4.70
	C	1.25	1.28	1.26	1.21
Pore diameter - 0.5 mm, Thickness - 5 mm	K	2.24	2.46	3.46	3.37
	C	1.32	1.45	1.79	1.75
Pore diameter - 0.4 mm, Thickness - 5 mm	K	1.49	1.42	1.76	1.76
	C	2.16	1.91	2.28	2.26

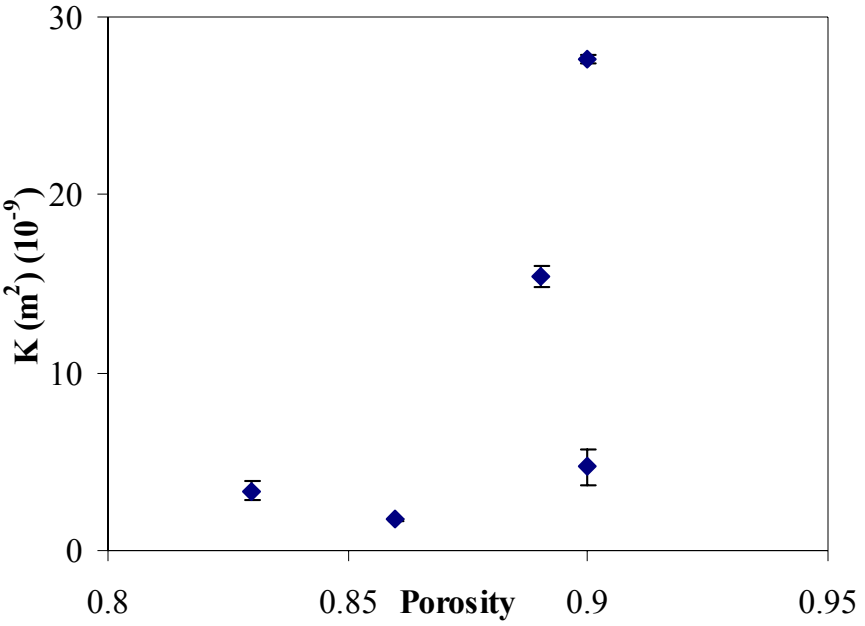

Figure 4.12: K versus Porosity for various RMF

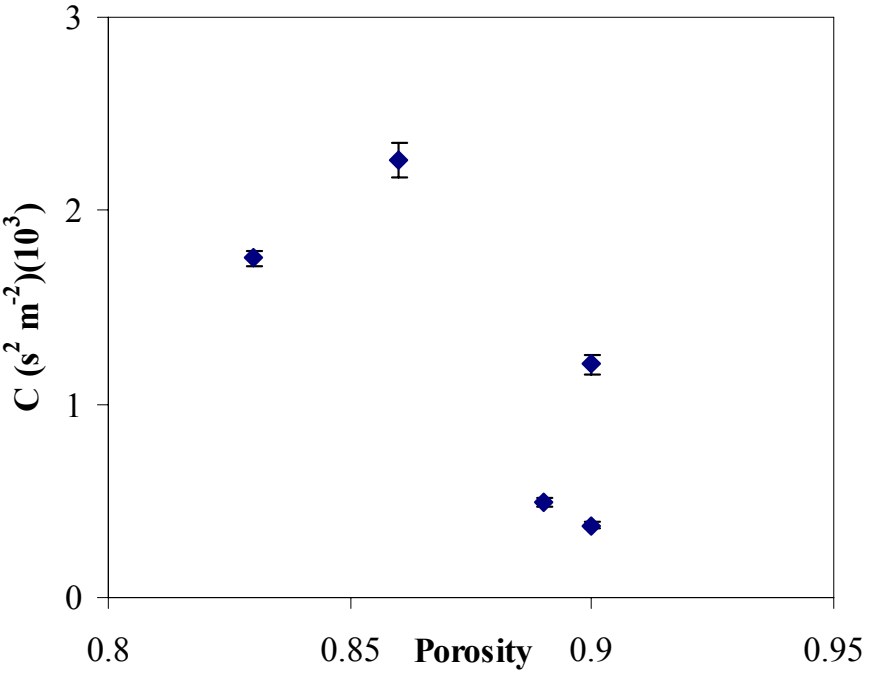

Figure 4.13: C versus Porosity for various RMF

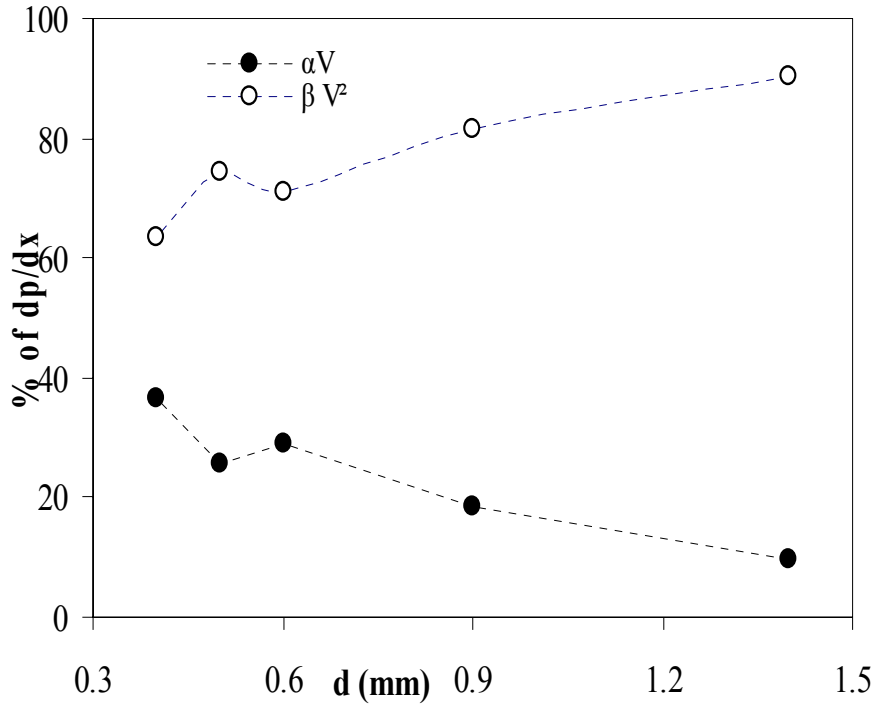

Figure 4.14: pressure drop contribution from two terms of the equation 2.5

Figure 4.14 shows that the pressure drop contribution from the quadratic term of equation 2.5 is large compared to Darcian velocity term. For pore diameter 1.4 mm, this contribution is more than 80 %. As the pore size increases the quadratic term's contribution to pressure drop increases. This suggests that the quadratic term's contribution is predominant not only at higher velocity, but at lager pore diameter as well.

4.1.2 Model versus experimental results

A direct approach to find a relationship between the various properties of porous media is by means of establishing empirical correlations [39, 41]. From the literature, it is clear that general relationship between porosity or pore diameter and permeability can not exist. Experimental results are evaluated with widely accepted quadratic model of Hazen-

Dupuit-Darcy. Some basic assumptions were made such as no pores are sealed off, pores are reasonably uniform in size and fluid motion occurs like motion through capillaries. Figure 4.15 shows K values for different pore diameter using equation 2.9 for RMF. It can be seen that, K increases with the increasing average pore diameter. The K and C (Figure 4.16) values were calculated using equations 2.9 and 2.10 based on the pressure drop data measured for 3 replicas of each grade of RMF samples. Values of *A* and *B* used in equations 2.9 and 2.10 were 100 and 1.0, respectively. These values lie within the intervals obtained by Tadrist and Miscevic [32], from 100 to 865 for constant A and 0.65 to 2.65 for constant B. Tadrist and Miscevic obtained the limits for constants A and B by experimenting various kinds of porous structures. Experimental results of the RMF are in agreement with the model suggested by Tadrist and Miscevic. This model is Ergun-like model, which is derived from Hanzen-Dupuit-Darcy equation.

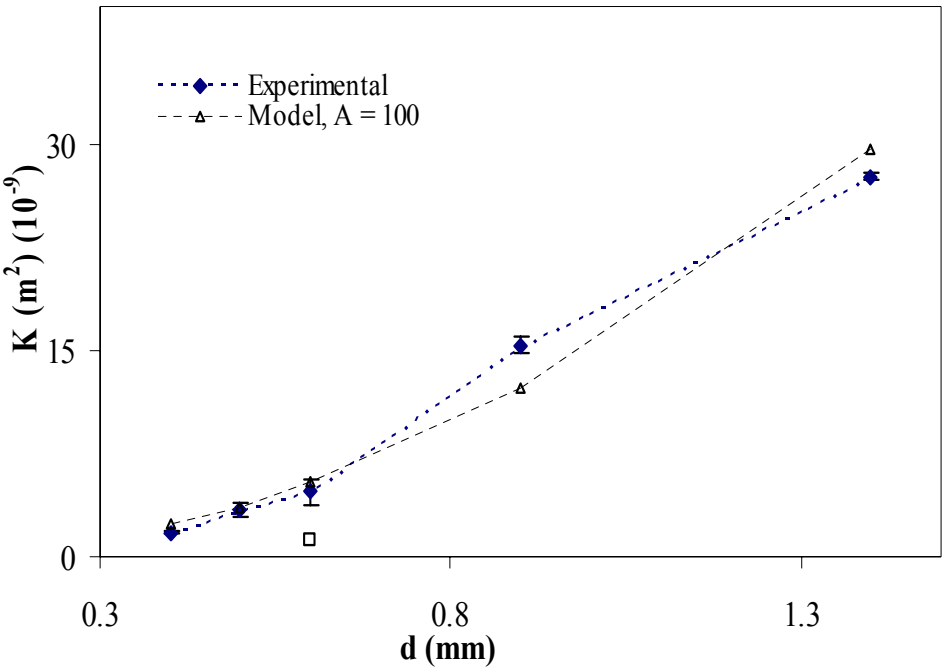

Figure 4.15: Permeability: Model versus Experimental.

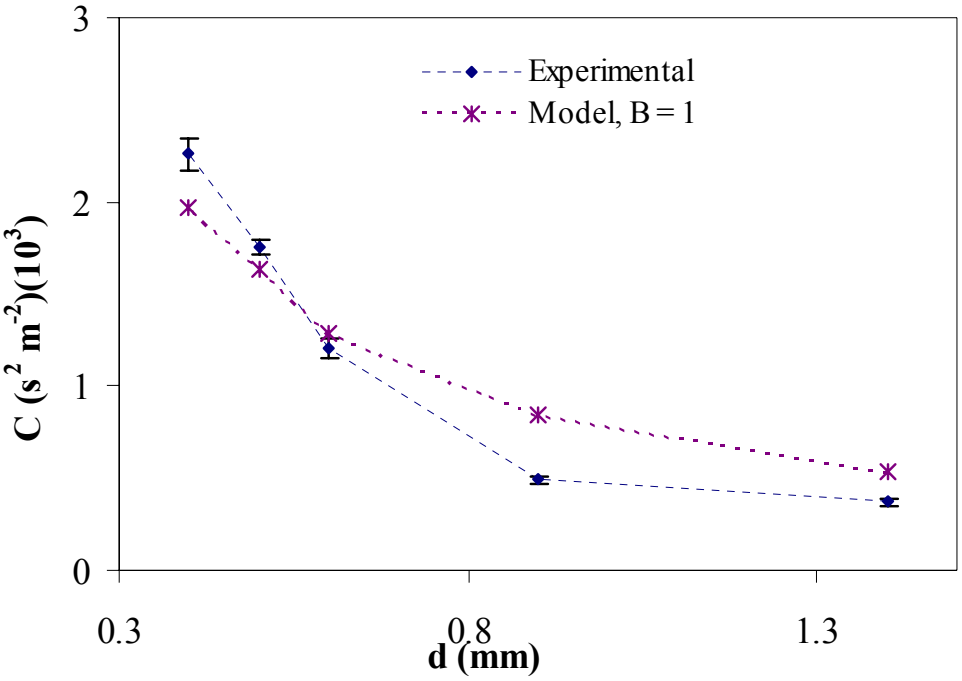

Figure 4.16: Non Darcian Permeability Cœfficient: Model versus Experimental.

4.1.3 IMI metal foam results

Pressure drop was measured for all the samples of IMI metal foam. IMI metal foams were available in two different morphologies. Figure 4.17 shows the unit pressure drop measured against all velocities for Ni70-1A3 and Ni60-1A2. Pressure drop for all the Ni70 samples was found to be much higher than any Ni60 sample, although the average pore diameter for Ni60 is smaller than that of Ni70. An attempt to explain this observation will be discussed in this section.

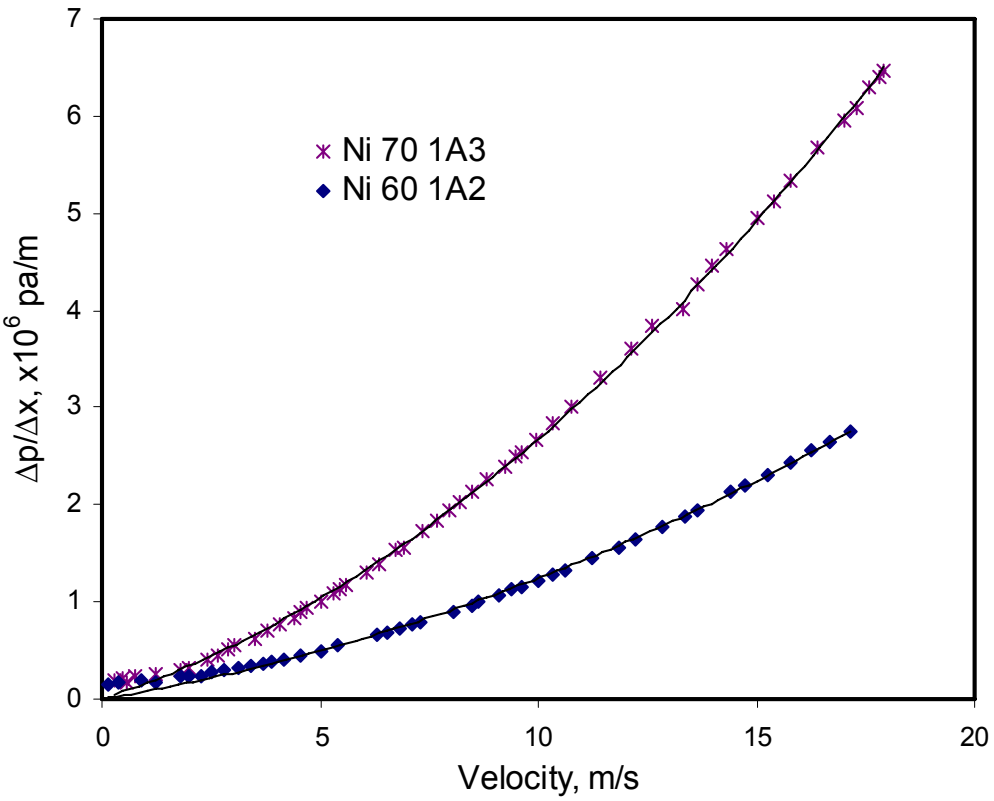

Figure 4.17: Unit pressure drop versus Velocity for Ni70-1A3 and Ni60-1A2 samples.

Table 4.3 lists the permeability and drag coefficients for IMIMF. The averages of K for thinner sample (dx=8.54) and thicker one (dx=11.55) are $2.38 \pm \frac{0.10}{0.27}$ and $1.59 \pm \frac{0.10}{0.07}$, respectively. The Ni60 samples showed higher permeability value, with similar variation within the same sample set than Ni70 samples. Coefficient C for Ni60 and Ni70 samples are $4.15 \pm \frac{0.54}{0.45}$ and $8.73 \pm \frac{0.26}{0.22}$, respectively. It can be seen that C increases with decreasing the thickness. K and C were calculated for different velocity ranges as shown in Table 4.4. It can be seen from this table that K and C values depend on the velocity range.

Table 4.3: Quadratic curve coefficients (α and β), K (m^2) and C (m^{-2} s^2) for different IMI metal foams.

Average Thickness (dx)	Sample	Actual Thickness	$\alpha = \mu / K$	$\beta = \rho.C$	R^2 %	K ($\times 10^{-10}$)	C ($\times 10^3$)
11.53mm	Ni70-1A3	11.80	116732	10666	99.92	1.58	8.70
	Ni70-1A4	11.40	121420	10431	99.91	1.52	8.51
	Ni70-1A5	11.40	109069	11034	99.95	1.69	9.00
8.48mm	Ni60-1A2	8.38	74524	4988.4	99.61	2.48	4.07
	Ni60-1A3	8.80	87837	5764.5	99.58	2.11	4.70
	Ni60-1A4	8.27	72477	4544.4	99.41	2.55	3.70

Table 4.4: K m^2 ($\times 10^{-10}$) and C ($s^2 m^{-2}$) ($\times 10^3$) for IMIMF at different velocity range.

dx, mm		<5	<7	<10	<15	<17
11.55	K	1.37	1.57	1.71	1.69	1.61
	$(\text{Standard Error})_K$	0.07	0.06	0.06	0.07	0.07
	C	3.39	7.43	9.07	8.99	8.56
	$(\text{Standard Error})_C$	0.67	0.49	0.36	0.25	0.24
8.54	K	1.70	1.70	1.93	2.40	2.35
	$(\text{Standard Error})_K$	0.06	0.07	0.06	0.09	0.094
	C	-	-	2.35	3.85	4.281
	$(\text{Standard Error})_C$			0.27	0.19	0.24

Figures 4.18 and 4.19 show that the values of K for Ni70 MF are lower whereas values of C are higher for all the velocity ranges. Variation of C for Ni60 MF is not as high as Ni70 MF. The plot indicates that there is an optimum velocity range, in which, K is maximum. For 11.55 mm and 8.54 mm thick samples, R^2 values vary for the different velocity ranges from 91 - 98 % and 94 - 99 %, respectively. However, the non-Darcian coefficient (C) increases significantly with the increase in fluid velocity. Higher K values for Ni60 samples indicate that they were more permeable and that their pressure loss due to the quadratic term of equation 2.6 was less dominant when compared to Ni70 samples. As proposed by Lage [18], the transition from linear (viscosity-dominated flow) to quadratic (inertia-dominated flow) regime is medium-specific. Indeed, as shown in Figure 4.19, Ni60 is in a Darcian flow regime at 5 m/s while Ni70 imposes a significant drag related to the geometry of the porous medium and/or inertia.

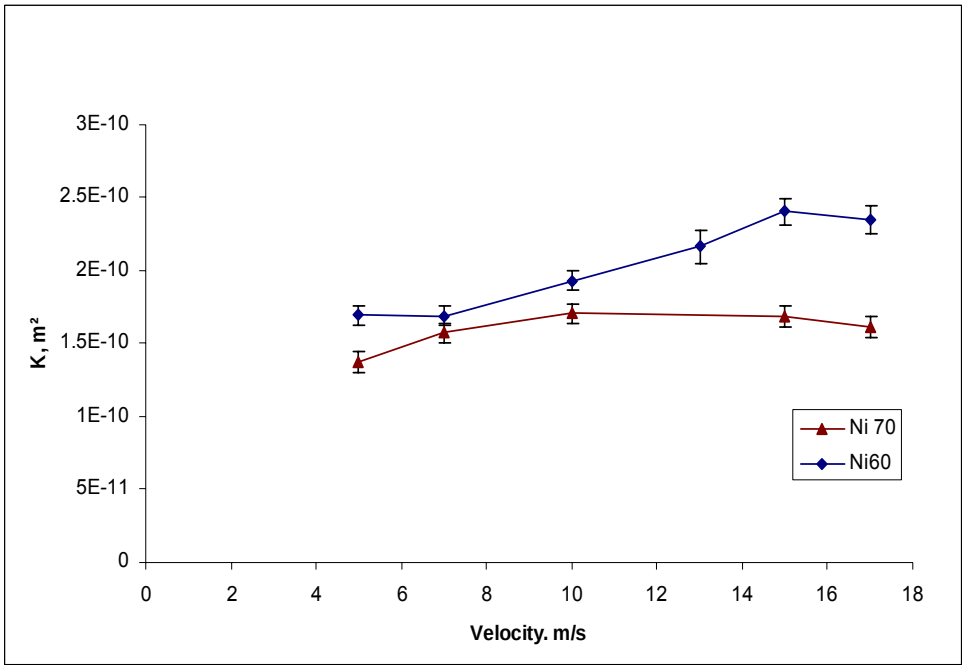

Figure 4.18: K versus velocity comparison for Ni70 and Ni60 samples.

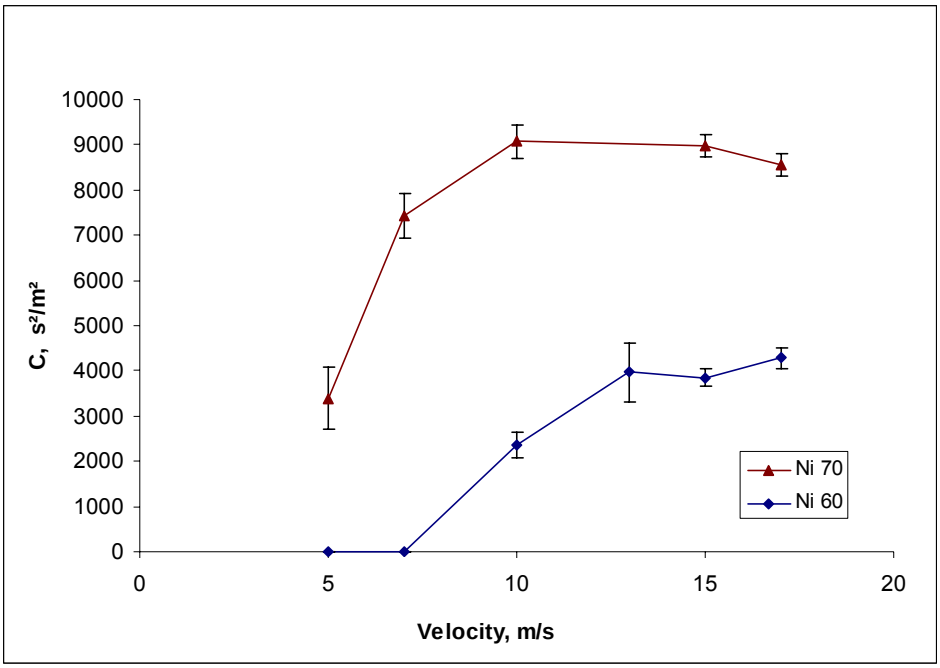

Figure 4.19: C versus velocity comparison for Ni70 and Ni60 samples.

The effect is better illustrated by Figure 4.20 where the relative contribution of the term ρCV^2 of equation 2.6 is shown as a function of fluid velocity. For both foams, Ni70 and Ni60, the drag force contribution increases with fluid velocity. For Ni60 foam, the drag force contribution is zero for velocity lower than 7 m/s. The balance between viscous and drag force contribution is related to the balance between: (1) the effective surface area and (2) the structure of the solid porous matrix (tortuosity). Therefore, the relative contribution of viscous force and drag force must depend on the internal geometry of the porous material. Through image analysis software, pore sizes and the window sizes were measured. Since pores are intricately structured, pores identification needs human interaction and hence readings could differ from person to person. Windows of some of the pores are not located normal to eye sight and look like elliptical

shape. In this case largest diameter of the pore or the window is taken as the actual size, assuming originally they are spherical or circular in nature.

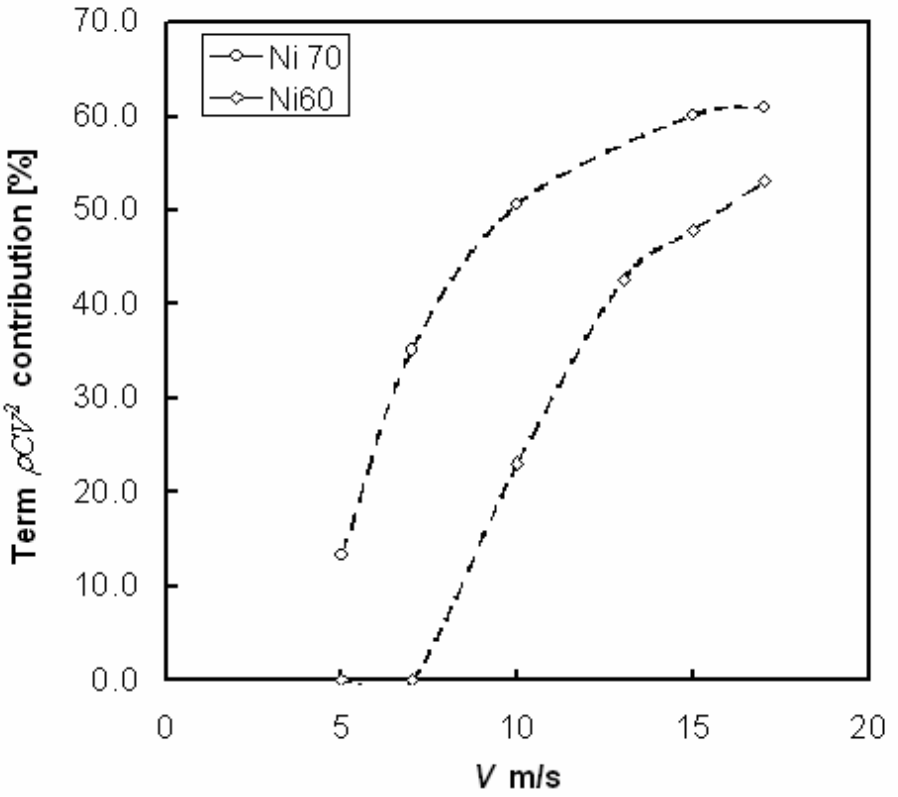

Figure 4.20: Effect of the fluid velocity on the relative contribution of the term ρCV^2 of equation 2.6 on the normalized pressure drop ($-\Delta P/\Delta x$) measured on both Ni70 and Ni60 samples.

Figure 4.21 shows one of such measurements for Ni60 sample. Averaged values of the pore size and windows size measurements were listed in Table 4.5. The average pore size for Ni70 and Ni60 were measured $486^{\pm 26}$ and $296^{\pm 23}$, respectively. The pore size of the two grades is significant different. The pore size of Ni70 is almost one and half times, on average, larger than Ni60 foam. Visual comparison of the SEM pictures of

the two different foams (Figures 4.23 and 4.24) shows this obvious difference between the pore sizes. However, there is not much difference between the windows size of the two different foams as can be seen in Table 4.5.

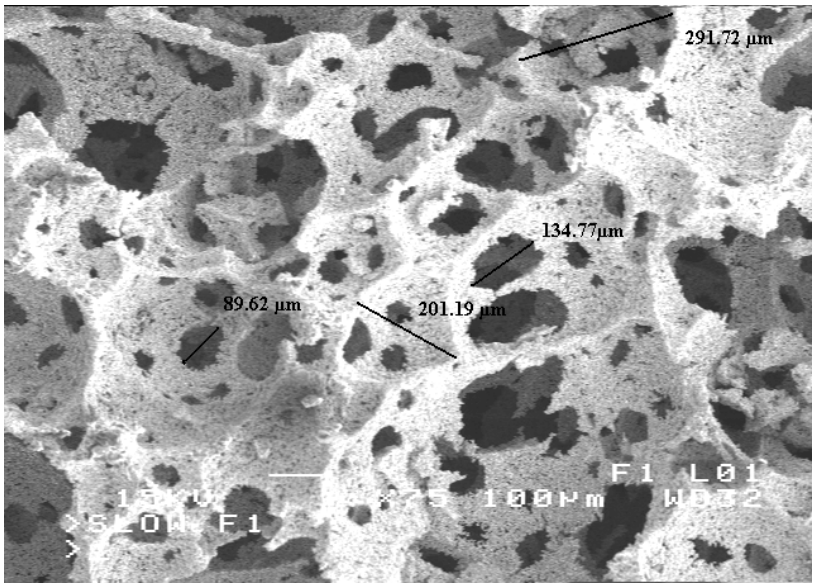

Figure 4.21: Image analysis for Ni60-1A2 at x75 magnification.

Table 4.5: Pore size, Window size for various IMI metal foams.

Sample	Pore size		Window size	
	µm	Standard Error*	µm	Standard Error*
Ni70-1A3	485.7	17.35	57.0	2.42
Ni70-1A4	461.5	26.39	57.2	2.38
Ni70-1A5	512.4	19.93	55.4	2.17
Ni60-1A2	307.6	21.41	54.0	3.52
Ni60-1A3	309.8	29.86	67.9	0.44
Ni60-1A4	273.2	24.34	56.3	1.32

* Standard Error = standard deviation / number of measurements$^{1/2}$

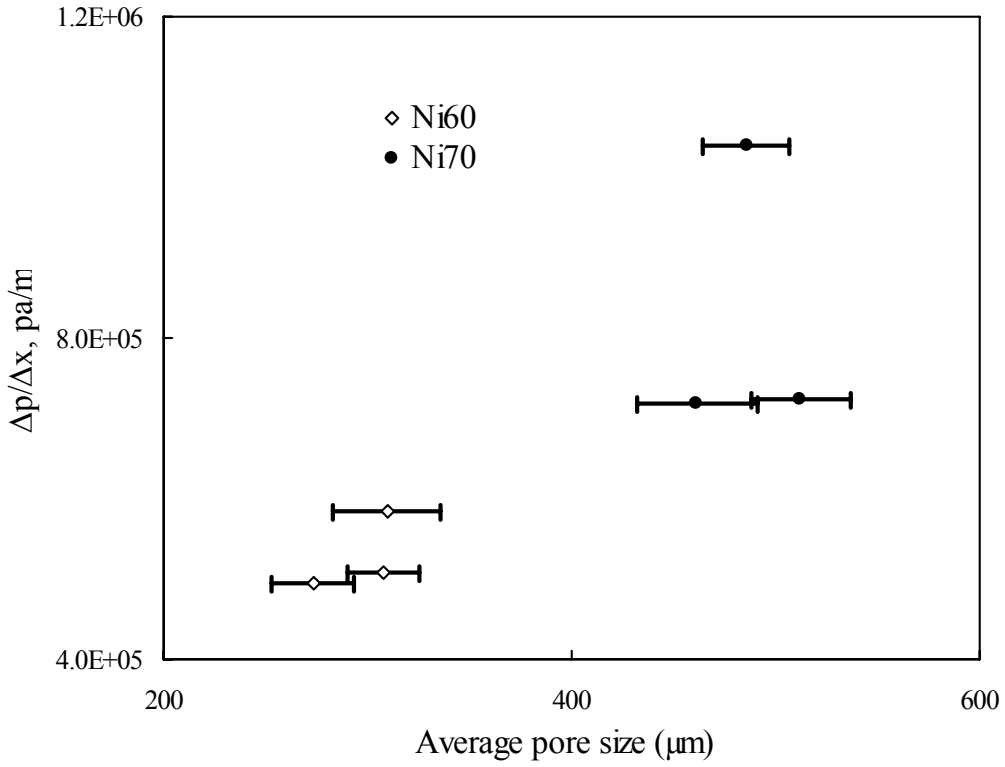

Figure 4.22: Pressure gradient (ΔP/Δx) measured at 5 m/s as a function of the average pore size.

Figure 4.22 demonstrates that pressure drop was lower for smaller pore diameter (Ni-60 samples) while, Ni70 samples measured higher pressure drop. This is contrary to what was expected. Figure 4.23 and 4.24 depicts the two different microstructures. SEM for both samples is done at the same magnification of x75 for measuring window size and at x25 for measuring pore size.

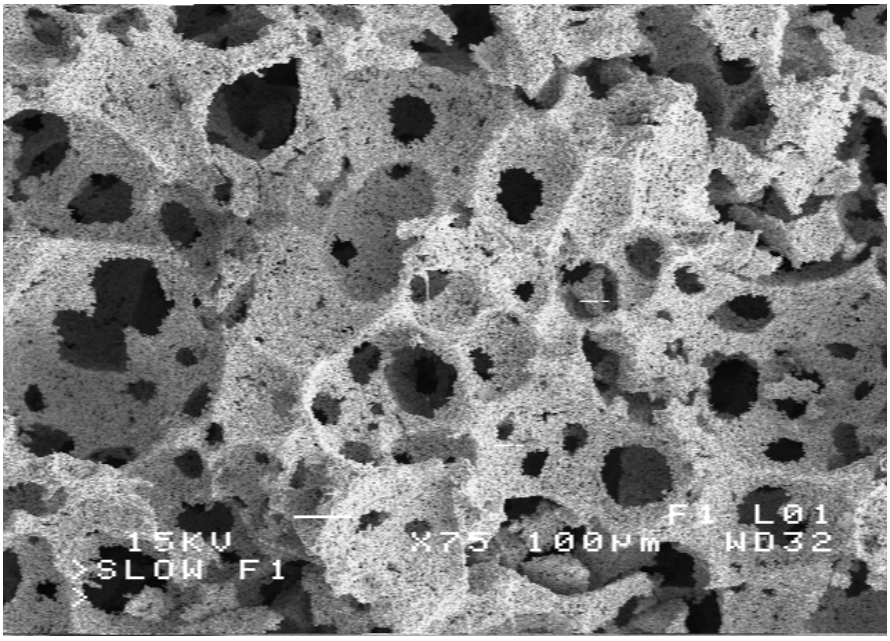

(a)

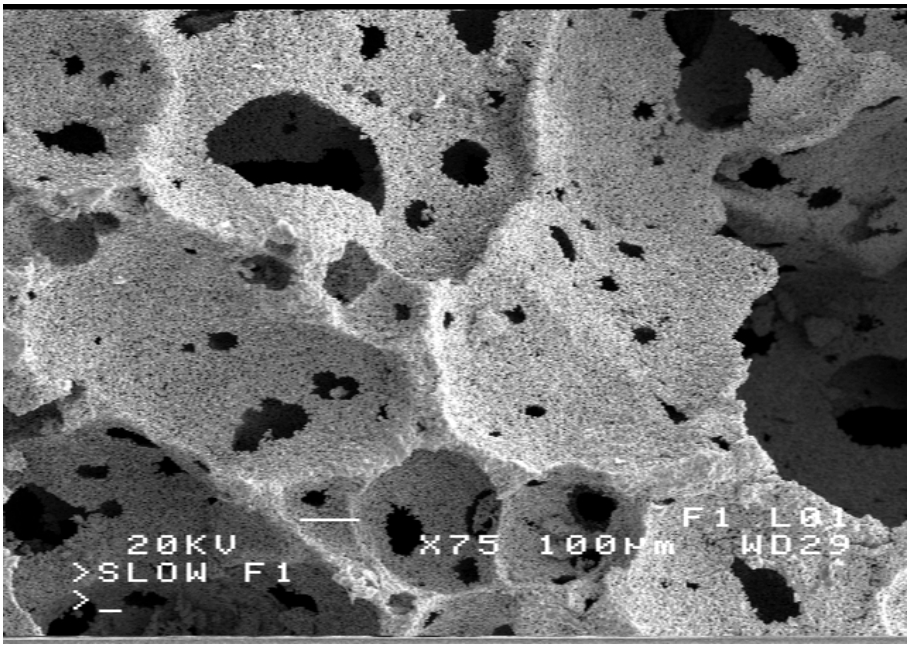

(b)

Figure 4.23(a): SEM picture Ni60-1A2 zone 5 at x75 (b): Ni70-1A3 zone 2 at x75.

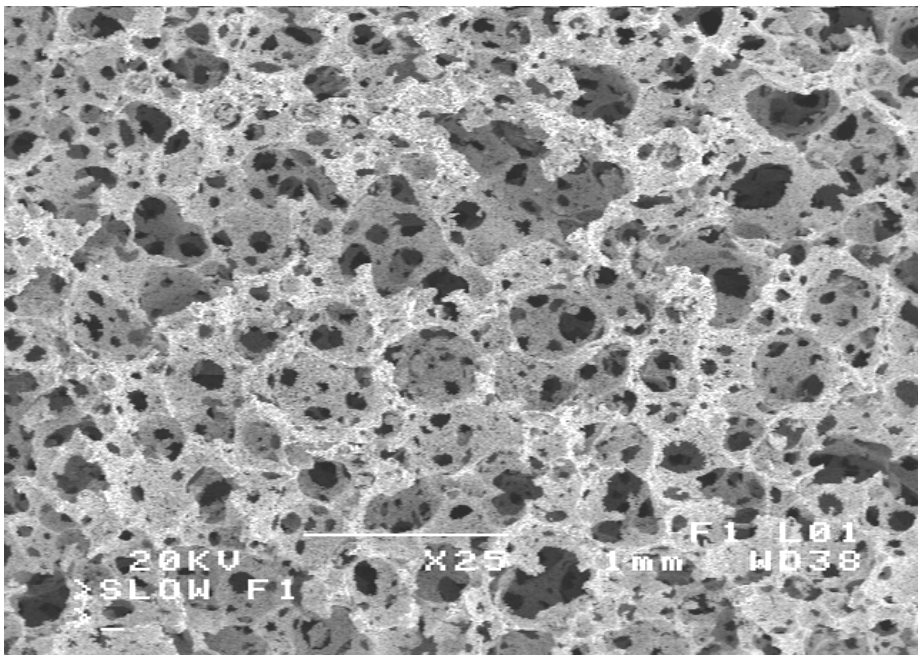

(a)

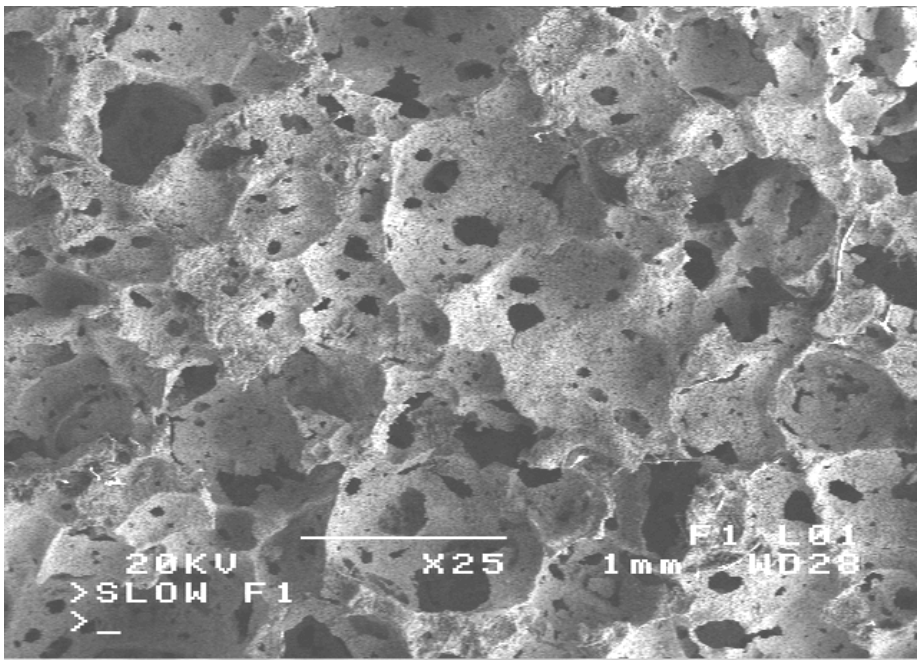

(b)

Figure 4.24(a): SEM picture Ni60-1A2 zone 1 at x25 (b): Ni70-1A5 zone 3 at x25.

From the micrographs in Figure 4.24, it can be seen that the number of pores in a given area is much less for Ni70 compared to Ni60. This suggests that, number of pores is more in Ni60, meaning, the number of windows is more, however, window sizes are measured to be almost same for both metal foams. This implies that, the open area for the flow of air through a particular section is more in the case of Ni60 compared to Ni70 samples. This reveals the main cause behind lesser pressure drop per unit length of thickness of sample Ni60 than that of Ni70, although pore size is bigger for Ni70 samples. This particular outcome was investigated further with sectioning over the thickness of the metal foam. Foam samples were machined in steps by removing layers of 0.5 to 1.5 mm thickness and air at pressure was blown to ensure sample is clean and no dust is left in the pores. At each step pressure drop and microstructure data were collected. Pressure drop for various thicknesses of Ni70-1A4 sample is given in Figure 4.25.

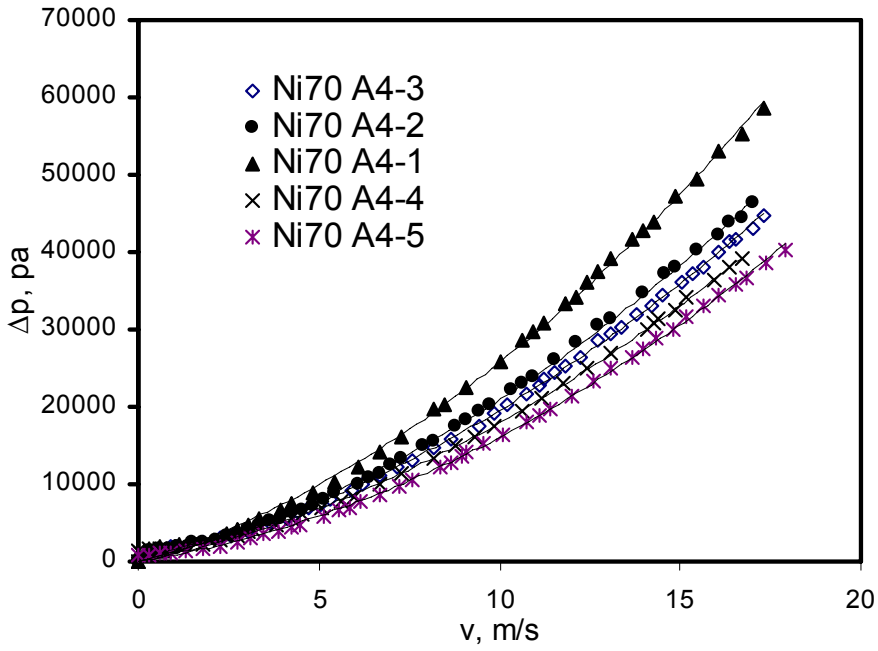

Figure 4.25: Pressure drop for various thicknesses of Ni70-1A4 sample.

Sample Ni70-1A4-1 has the largest thickness and Ni70-1A4-5 has the smallest, giving highest and lowest pressure drop, respectively. In each curve, value of R^2 is almost 100% that shows the proportional correlation of pressure drop to flow velocity of air. Table 4.6 lists the thicknesses of the sample after each machining step.

Table 4.6: Thickness reduction performed on the samples. All the dimensions in mm

Sample	***Thickness 1***	***Thickness 2***	***Thickness 3***	***Thickness 4***	***Thickness 5***
Ni60-1A2	8.38mm	-	-	-	-
Ni60-1A3	8.8 mm	8.25 mm	-	-	-
Ni60-1A4	8.27 mm	7.75 mm	-	-	-
Ni70-1A3	11.8 mm	10 mm	9.3 mm	8.64 mm	8 mm
Ni70-1A4	11.4 mm	9.92 mm	9.3 mm	8.76 mm	8.2 mm
Ni70-1A5	11.4 mm	9.9 mm	9.2 mm	-	-

Figures 4.26 and 4.27 show the unit pressure drop for various thicknesses of samples Ni70-1A4 and Ni70-1A3, respectively. From these figures, it is evident that unit pressure drop is not constant for most of the thicknesses, this is more noticeable in Figure 4.25 of Ni70-1A4 sample.

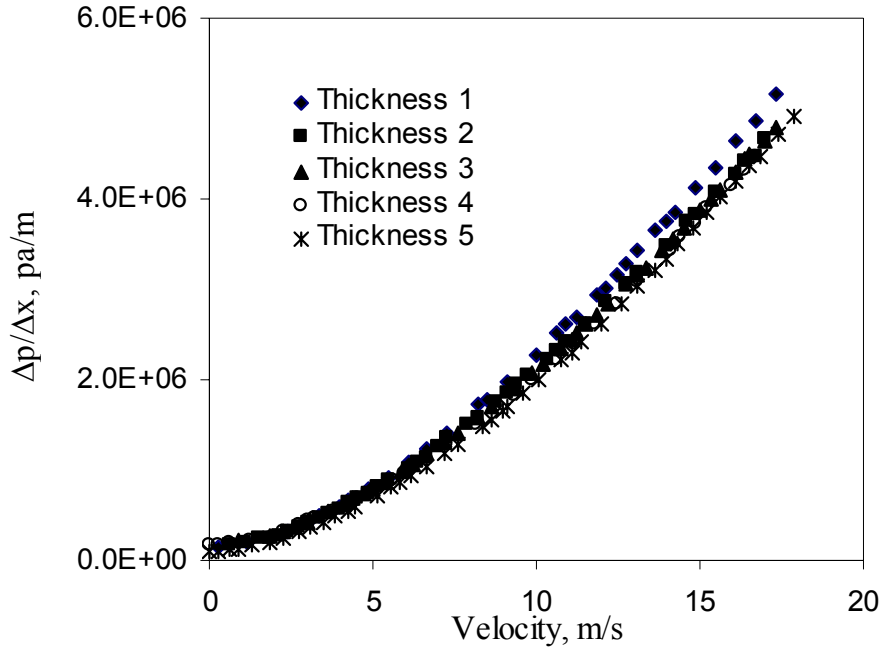

Figure 4.26: Unit pressure drop versus velocity for various thicknesses of Ni70-1A4 sample.

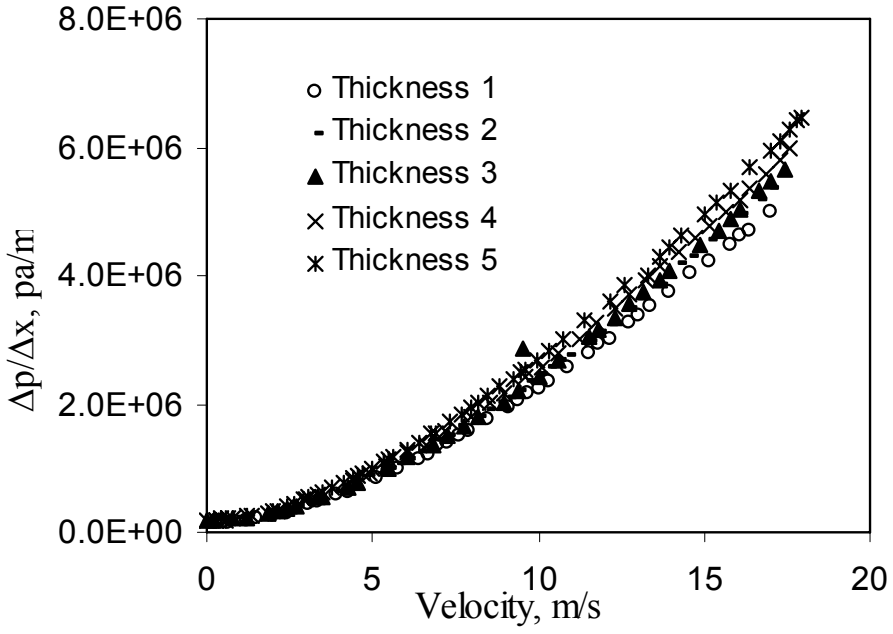

Figure 4.27: Unit pressure drop versus velocity for various thicknesses of Ni70-1A3 sample.

For Ni70-1A4 (Figure 4.26) except thickness 1 pressure drop data for other thicknesses lie on the same quadratic line, while for Ni70-1A3 (Figure 4.27) separate quadratic lines could be seen for most of the thicknesses. This means some of the layers which were machined off were not homogeneous with the rest of the layers. This could also been seen in Figure 4.28. This figure presents the pressure drop recorded at different thicknesses for various IMIMF samples.

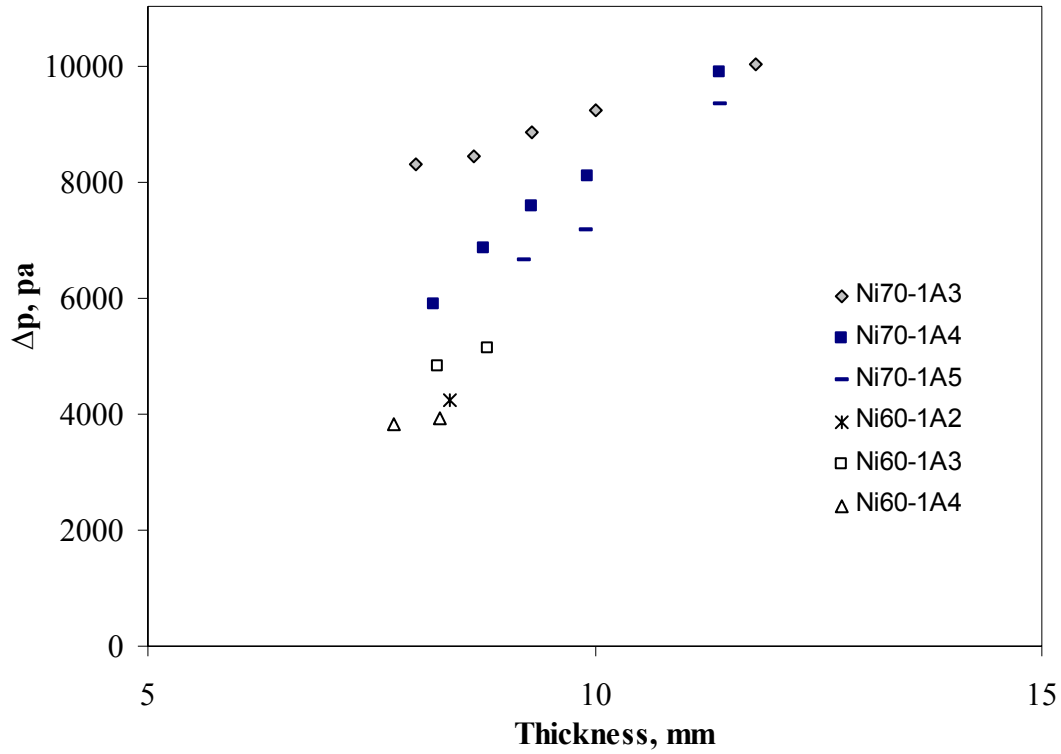

Figure 4.28: Pressure drop for nickel samples at different thicknesses at 5m/s.

From this figure, all the samples of Ni60 measured lower pressure drop compared to Ni70 samples. Linear curve could be drawn for Ni70-1A4 sample data points, while some of the points offset with linearity for Ni70-1A3 sample. However, these curves do not pass through zero coordinates. This means that the layers that were machined for

Ni70-1A4 sample were homogeneous with each other, while the rest of the sample or some part of the sample is not homogeneous with those layers. While in case of Ni70-1A5 sample, since some of the points deviate from linearity, discrete lines could be drawn among those points, an indication of variation in microstructure among layers. Eventually if these curves have to pass through zero coordinate, pressure drop per unit length would be high for Ni70-1A3 compared to Ni70-1A4 sample. Reasons behind this ambiguity could be investigated by interpreting pressure drop for each layer. Factors that are affecting pressure drop for each individual layer are studied. Hence, each layer machined is regarded as one sample, therefore, microstructure of the individual layers is studied in greater detail.

As discussed before SEM pictures of the surface of IMIMF were taken at five different zones. Open area for the flow of air was measured for all these individual zones and then added. These readings are given in Table 4.7. Pressure drop for the particular

Table 4.7: Pressure drop, open area to the flow of air and thickness of individual layers.

Sample	Pressure drop, pa	Open area, μm^2	Thickness, mm
Ni 70-1A5	508.93	725039.8	0.70
Ni 70-1A3-4	390.00	675991	0.66
Ni 70-1A4-4	720.93	450280	0.54
Ni 70-1A3-5	169.17	869758.2	0.64
Ni 70-1A4-5	994.3	367869.9	0.56
Ni60-1A3	310.08	1217415	0.55
Ni60-1A4	105.52	945122.6	0.52

layer is calculated by means of mathematical subtraction of the pressure drop before machining and that after machining.

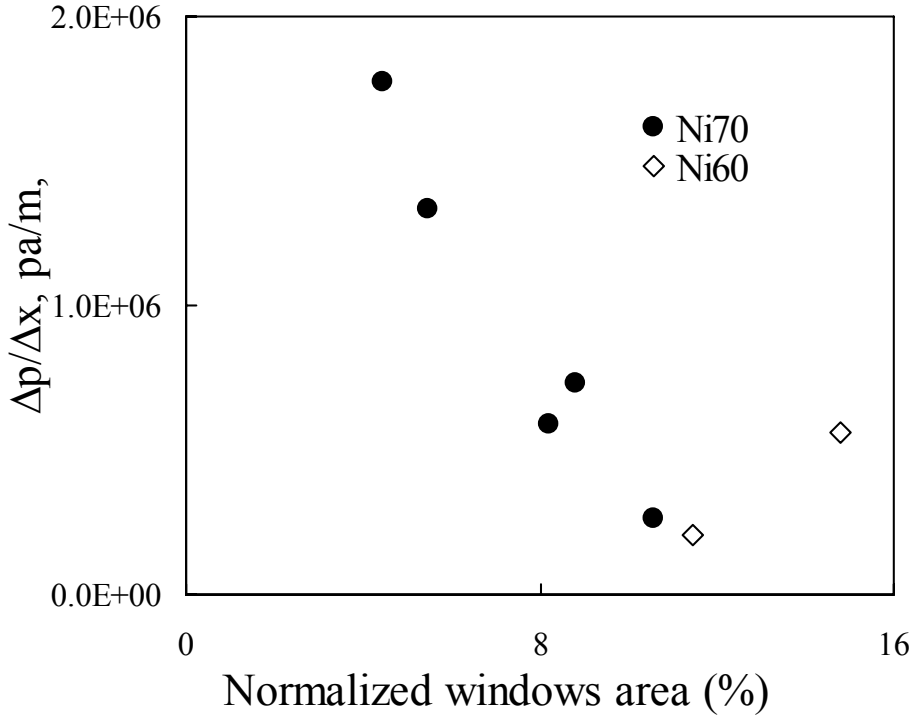

Figure 4.29: Unit pressure drop measured at 5m/s as a function of normalized window area (The total area of the windows divided by the examined area 8.24mm^2)

From Figure 4.29, it is apparent that as the open area to flow of air through the metal foam layer increases, the pressure difference across that layer decreases. Although, the pore diameter in Ni70 is greater than in Ni60, the open area to the flow is smaller and this causes larger pressure drop across the foam thickness. The wall of the pores creates resistance to the flow of air and hence it is clearer that mere pore size difference of the metal foams do not affect the pressure drop. In another independent test composite of two discs of Ni70-1A3 and Ni60-1A4 was prepared. Pressure drop data was collected at

various velocities and again for the same range of velocity after alternating the order of discs. That is, in the first case Ni60-1A4 disc was facing the flow and in the second case Ni70-1A3 disc facing the flow. The results of this test are shown in Figure 4.30.

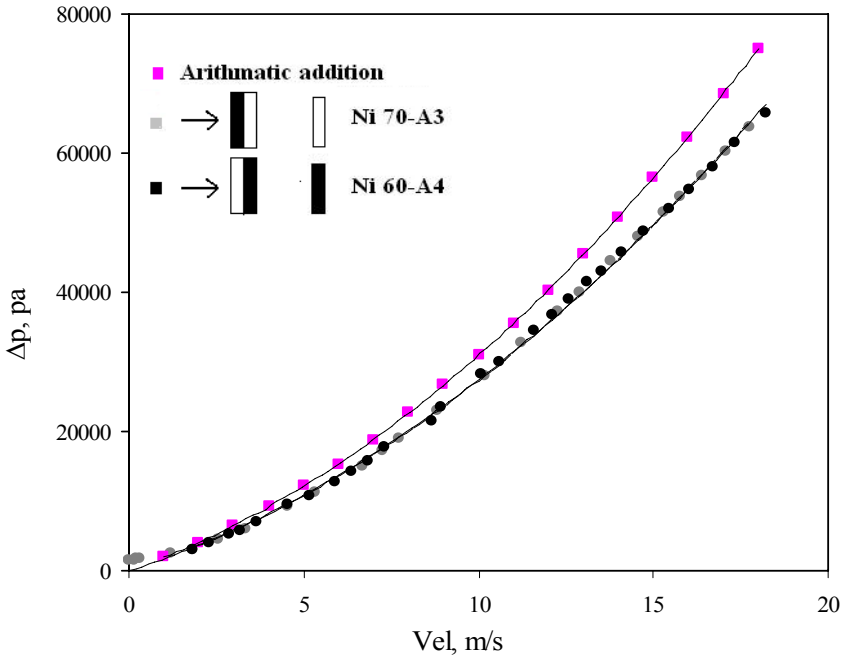

Figure 4.30: Pressure drop versus velocity for composite.

Figure 4.30 shows that alternating the order of discs did not affect the pressure drop behavior of the composite. While, by mathematically adding the pressure drop for the individual disc resulted in higher pressure drop. This difference is quite noticeable and is an evidence of pressure drop due to inertia. The fact is when air impacts the surface of the metal foam there is a sudden change in momentum causing pressure loss. In the case of mathematically adding pressure drop for individual samples, this loss was counted two times. While in the composite case, the pressure drop due to a sudden impact was counted only once.

From porosity measurements, average porosities for three replicas of Ni60 and Ni70 are 94.2 % and 92 %, respectively. This means that the volume fraction of the voids in Ni60 is higher than that in Ni70. Figure 4.31 represents porosity versus unit pressure drop at 5 m/s for various IMI metal foams. As the porosity decreases unit pressure drop increases or the permeability decreases, except between porosity point 92.2% and 92.7%, where there is a slight increase in pressure drop.

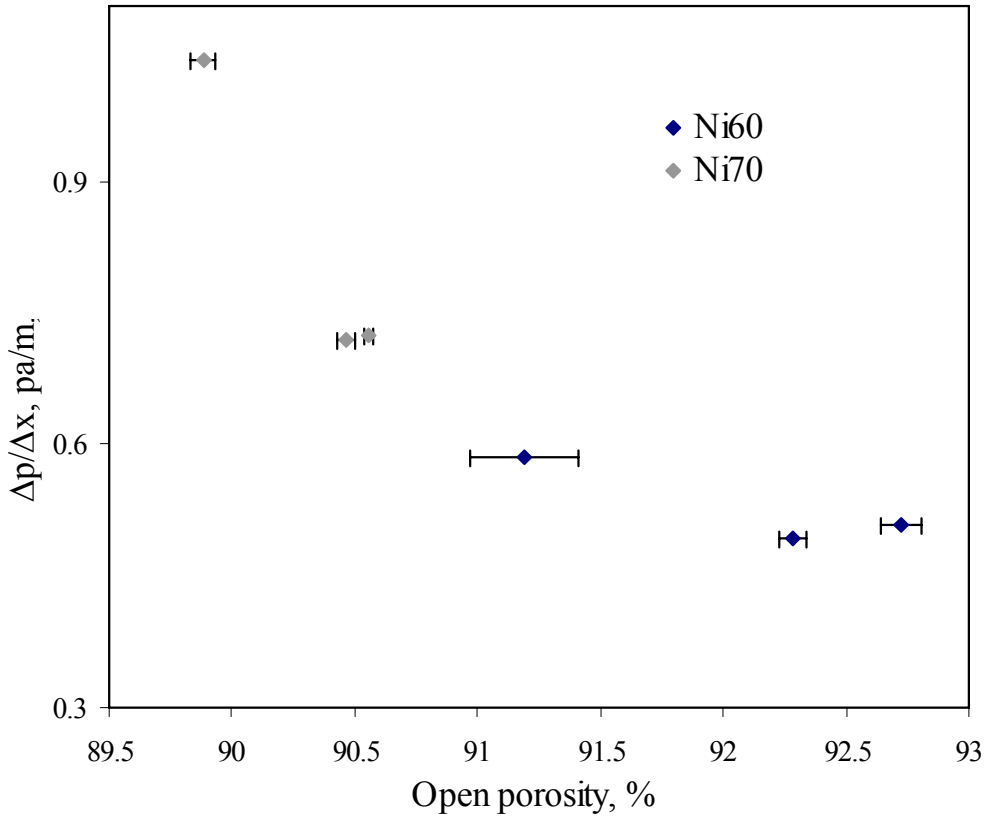

Figure 4.31: Unit pressure drop versus Porosity at 5m/s.

Permeability of Recemat and IMI samples were also compared with the model suggested by Despois and Mortensen [39]. Figure 4.32 shows the combined effect of pore

size and porosity on the permeability and a comparison with Despois and Mortensen model. The model predicts the general trend for both IMIMF and RMF but higher values than those of IMIMF and lower values than those of RMF samples. This suggests that there are other morphological parameters which need to be included for accurate prediction of the permeability. Moreover, Despois and Mortensen had made assumptions, such as, the model is based on the average size of the windows and there is one "active window" per pore, these might not be valid for the foams studied here. More importantly, this model is valid only for the Darcian velocity range hence quadratic term is neglected.

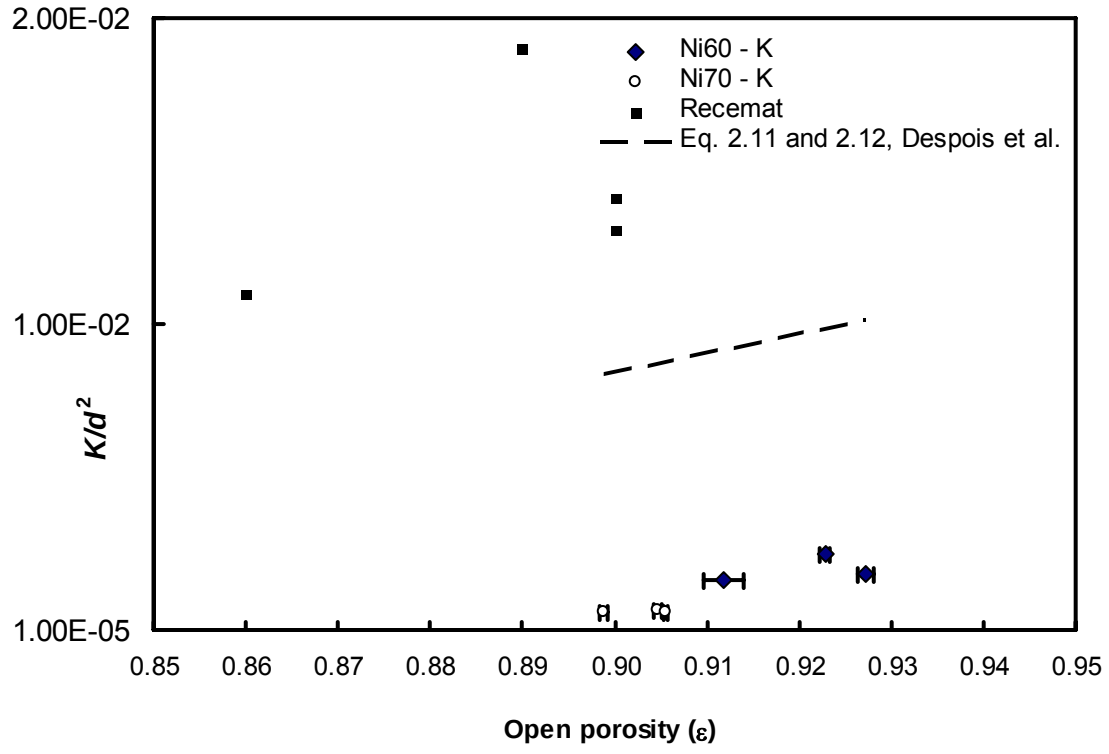

Figure 4.32: Effects of the foam porosity on the permeability (K) normalized by the pore size squared (d^2) compared to the model of Despois and Mortensen [39].

CHAPTER 5

SUMMARY, CONCLUSIONS, RECOMMENDATIONS FOR FUTURE WORK AND CONTRIBUTIONS

5.1 Summary

Metal foam has important industrial applications, which require better understanding of their permeability. Large amount of work has been done so far to define the pressure drop across the metal foam in terms of structural characteristics. Moreover, various inferences were made and analytical models were suggested in the past [13, 14, 18, 27, 29, 32, 33, 36, 41], which were not in agreement with each other. Most of the studies have therefore been directed towards experimental measurements. The aim of present work was to categorize various structural parameters responsible for the measured pressure drop across the porous media. Necessary equipment was built following the experimental set-up by Paek *et al.* [33] and ISO4022-1987-10-01 standards. Samples were tested for repeatability and hysteresis.

The Recemat and IMI metal foam samples made from metallization of polyurethane foam by electro-discharging and powder metallurgy approach, respectively. The former has well distributed and uniform pore structure, while the latter could be produced in mass but at the expense of non-uniformity of the cell structure. Nevertheless, IMI foams have the advantage of low cost. Some of the structural properties of Recemat metal foam were provided by the manufacturer like pore size and pores per inch, however, porosity was measured by following ASTM-792-98 standards. For the IMI

samples, porosity was calculated from data obetained using gas pycnometer. SEM micrographs were acquired to measure pore diameter and window size.

Pressure drop data at various velocities for various Recemat samples was recorded. These values were averaged from three replicas of each grade. For fully developed Newtonian fluid flow, the permeability and non-Darcian coefficient were determined for each sample using the velocity range of 0 m/s to 20 m/s by curve fitting procedure. Fitting the data in 3rd order curve slightly improves R^2 value, but suggesting that it is cubic in nature [27] would not be entirely correct. Pressure drop measured found to increase as pore size decreases. Moreover, as pore size increased, permeability constant K increased and non-Darcian permeability coefficient, C decreased. However, no linear relation could be seen, as suggested by Innocentini *et al.* [41-42] in a study of gas flow through ceramic foam. These results are in agreement with the preceding researchers suggestions. For example, Flourie *et al.* [37] found that as the pore count per inch decreases, pressure gradient decreases. As well, Bhattacharya and Mahajan [14], experimentally demonstrated the increase in permeability with pore size. More recently, Tadrist and Miscevic [32] found that their experimental data agreed well with an Ergun-like law, which is pore dimension based. However, IMI metal foams did not show this trend, a big difference in pressure drop behavior was found for two different pore diameter samples. Ni70 samples have larger pore diameter whereas it recorded large pressured drop, while Ni60 samples showed higher permeability values. This is not expected. Moreover, for the same pore diameter (d = 0.6 mm) Recemat metal foam, 5 mm and 10 mm thick samples showed only slightly different values of permeability ($4.70*10^{-9}m^2$ and $4.93*10^{-9}m^2$, respectively). This indicates that the increasing thickness

of the MF has marginal effect on K and C. This is probably due to uniform morphology of the metal foam over the length. Whereas, IMI metal foams were obviously not homogeneous over the thickness. To study this, sectioning over the length of the metal foam was performed and each layer was studied in details. Pore size for Ni70 and Ni60 was measured as $486^{\pm 26}$ and $296^{\pm 23}$ μm, respectively.

For Recemat samples, permeability constant, K and non-Darcian coefficient, C did not vary significantly over the tested velocity ranges. As suggested by Antohe *et al.* [27], K and C are not flow rate dependant but both coefficients are shown to be velocity range dependent. For IMI metal foams, the effect of velocity of flowing media had less impact on the values of K. For Ni70 samples, it was found to be within the range of 1.47 to $1.74*10^{-10}m^2$ and for Ni60 samples within 1.72 to $2.38*10^{-10}m^2$. However, non-Darcian coefficient, C, increased with the velocity of flowing media. For Ni70 samples, C varied between 5.265 and $9.605*10^3$ s^2/m^2 and for Ni60 samples, the values were between 0 and $4.28*10^3$ s^2/m^2. Higher K values for Ni60 samples show that they are more permeable while pressure loss due to quadratic term in equation 2.5 was less dominant compared to Ni70 samples. As explained by Diedericks and Du Plessis [30], coefficient *C* is important and becomes significant as the flow velocity increases. As proposed by Lage [18], the transition from linear (viscosity-dominated flow) to quadratic (inertia-dominated flow) regime is medium-specific. For nearly same pore diameter of IMI and Recemat samples, the value of coefficient C of IMIMF was found much higher than that of Recemat. This difference in behavior of the Recemat and IMI samples is obvious, since pores of IMI samples had wide walls which created extra flow resistance to flow of air.

For RMF, the pressure drop contribution from quadratic term is large compared to Darcian velocity term. For pore diameter 1.4 mm, its contribution is more than 80 %. As the pore size increases, the quadratic terms contribution to pressure drop increases. This suggests that the quadratic term is predominant not only at higher velocity, but at lager pore diameter as well. This is also true for IMIMF where contribution of quadratic term for Ni70 samples is more than Ni60 samples. For IMIMF, as the flow velocity increases this contribution increased significantly, which is obvious. This contribution may be due to the combined effect of drag and inertia force.

There is limited work in the literature that has included non-Darcian permeability data. This is may be because of using simplified permeability equation like Darcian law. Non-Darcian permeability represents the inertial energy losses during air flow within the porous medium, which highly depends upon $\rho.v^2$, which is the kinetic energy. Impact of flowing fluid on the porous medium has to be understood in detail in respect to the friction with the solid part of the medium. When flowing media speed increased within metal foam, energy losses will be mainly due to the kinetic energy as explained by Innocentini *et al.* [41]. This is validated in another independent test of composite made of two very different morphologies of IMI samples. As discussed in section 4.1.3, composite measures less pressure drop than adding mathematically the two individual pressure losses. Several researchers interpreted the meaning of the quadratic term of equation 2.6 in different ways. For instance, Lage [18] argued that fully developed steady flow has zero inertia, which is partially true since before reaching to fully developed state there is change in velocity. While many researchers [21, 29, 40] supported the fact that the quadratic term of the equation is due to inertia of the flowing media. Moreover, in the

case of composite, the change in the order of the discs does not affect the pressure loss. Although, the two discs have two different morphologies, change in the morphology of the facing surface to the flow of air had no impact on the resultant pressure drop. For this study, it is clear that higher values of quadratic term of the equation 2.6 is from inertia and may be due to a contribution from the drag force exerted by the porous structure.

From porosity measurements, average calculated porosities for three replicas of Ni60 and Ni70 are 94.2 % and 92 %, respectively. As reported by Paek *et al.* [33], the optimal ε is what corresponds to maximum permeability. Their value for optimal ε was 94% as shown in Figure 2.3 (a). However, since there is only one data point which showed drop in permeability in our case, it can not be considered as the optimal value of porosity for IMI foams. Besides, in recent studies by Bhattacharya and Mahajan and Boomsma and Poulikakos [14, 29], Figure 2.3 (b) shows that they did not find any optimal porosity. According to them, permeability of the porous media increases with increasing the porosity. Which is true since for given number of pores per inch, the fiber diameter decreases with the increase in porosity. As a result the open cross sectional area available for the flow of air in the pore increases, which reduces flow resistance. In IMI metal foam case, this is evident, as open area for the flow of air in the case of Ni70 samples is much smaller than that of the Ni60 samples. For Recemat metal foams the average porosity of the samples of pore size 1.4 to 0.4 mm was 0.90, 0.89, 0.90, 0.83, 0.86, respectively. Apparently, K shows no special trend with porosity. Tadrist and Miscevic [32], also, suggested that there is no clear correlation with porosity of metal foam.

For Recemat samples with the increase of pore diameter, K increases. The empirical constants A and B, lie within the interval obtained by Tadrist and Miscevic [32], therefore, experimental values found to be in close agreement with the model. Permeability of Recemat and IMI samples were also compared with the model suggested by Despois and Mortensen [39]. The model predicts higher values than those of IMIMF and lower than those of RMF samples. This suggests that there are other morphological parameters which need to be included for accurate prediction of the permeability. More importantly, this model is valid only for the Darcian velocity range hence quadratic term was neglected.

5.2 Conclusions

The main conclusions that can be drawn from the present work are:

(i) Pressure drop characteristics of IMIMF and RMF were found to fit a polynomial model of Hazen-Depuit-Darcy.

(ii) For the experimental conditions evaluated, the pressure drop observed in the metal foams is due to a combined effect of K (permeability) and C (non-Darcian permeability co-efficient).

(iii) For RMF specimens, permeability, K, increased whereas non-Darcian permeability, C, decreased with increasing pore diameter.

(iv) The effect of pore size on the permeability of IMIMF seems to be opposite to that observed with RMF specimens and on other porous medium reported by other researchers.

(v) The differences in K and C values between the two types of metal foams result from the differences in the microstructure of the foams.

(vi) The behavior of fluid flow in porous medium can be very complex. However, K and C could be predicted by Ergun-like model in RMF using appropriate A and B as suggested by Tadrist and Miscevic [32].

(vii) As the porosity increases, pressure drop decreases or permeability, K, increases, but the optimum porosity that corresponds to the maximum permeability could not be found for IMI metal foams.

(viii) For IMI metal foam, open cross sectional area for the flow of air is found to be the critical factor for pressure drop behavior or the combination of window size and numbers of windows have to be considered for predicting pressure drop.

(ix) Quadratic term of Hazen-Depuit-Darcy equation is mainly due to the inertia of the flow and partially may be due to the drag exerted by the microstructure of the porous media.

5.3 Recommendations for Future Work

a. The present work was limited to high velocity of flowing media, rather, experiments in Darcian velocity ranges need to be done to study the transition between Darcian and non-Darcian regimes.

b. IMI metal foam should be studied for wider range of samples of different pore diameters and porosities.

c. More SEM analysis should be performed in order to generalize open cross sectional area for predicting pressure drop for variety of morphologies.

d. Metal foams made for bio-medial applications (Ti foams) should be experimented.

e. More work should be directed to determine the different contributions of the non-Darcian pressure drop, i.e. drag and inertia forces, more precisely.

5.4 Original Contributions to Knowledge

- Equipment to characterize various metal foams has been designed and built at Concordia University. This equipment can be used to conduct further studies on metal foams or other porous media.
- The ambiguity over the existence of inertia force is eliminated in the present work.
- This research could be extended to study other foams of bio-medical interest, such as Ti, to understand their permeability behavior.

REFERENCES

1. Banhart, J. and Baumeister, J., "Deformation characteristics of metal foam", Journal of Materials Science, Vol.33, No.6, p1431-1440, 1998.
2. Banhart, J., "Manufacture, characterisation and application of cellular metal and metal foams", Progress in Material Science, Vol.46, No.6, p559-632, 2001.
3. Ashby, M. and Evans, A., "Metal foams a design guide", Butterworth-Heinemann, Oxford, UK, p251, 2000.
4. Benedyk, J., "Production and application of aluminum foam", Light Metal Age, Vol.60, No.3, p24-29, 2002.
5. De Wilde, A., Thijs, I. and Cooymans, J., "Method for producing metallic and ceramic products", European Patent EP1 329 438 A1, 2003.
6. De Wilde, A., Thijs, I. and Cooymans, J., "Method for producing metallic and ceramic foams", European Patent EP1 329 439 A1, 2003.
7. Shimizu, T., "Method for producing foamed inorganic powder", Japanese Patent JP2003027157, 2003.
8. Gauthier, M., Lefebvre, L., Thomas, Y., Bureau, M., "Production of metallic foams having open porosity using a powder metallurgy approach", Material and Manufacturing Processes, Vol.19, No.5, p793-811, 2004.
9. Vaidyanathan, R. and Fulcher, M., "Metallic, ceramic and cermet foam products and their methods of manufacture", US Patent WO 03/076109 A2, 2003.
10. Li, J. and Layrolle, P., "Porous metals and metal coatings for implants", US Patent WO- 02/066693 A1, 2002.
11. Scheidegger, A. E., "The physics of flow through porous media", 3rd edition,

University of Toronto Press, ISBN: 0-8020-1849-1, 1974.

12. Hudson, H. E. and Roberts, R. E., Proceedings - 2nd midwestern conference, Fluid Mechanics Engineering Series, Vol.31, No.3, p105, 1952.

13. Calmidi, V.V., "Transport phenomena in high porosity metal foams", Ph.D. Thesis, University of Colorado, Boulder, CO, 1998.

14. Bhattacharya, A. and Mahajan, R. L., "Thermo-physical properties of high porosity metal foams", International Journal of Heat and Mass Transfer, Vol.45, No.5, p1017-1031, 2002.

15. Bhattacharya, A. and Mahajan, R. L., "Finned metal foam heat sinks for electronics cooling in forced convection", Journal of Electronic Packaging, Vol.124, No.3, p155-163, 2002.

16. Phanikumar, M. S. and Mahajan, R. L., "Non-Darcy natural convection in high porosity metal foams", International Journal of Heat and Mass Transfer, Vol.45, No.18, p3781-3793, 2002.

17. Division of Engineering, "Porous material", http://www.cmse.ed.ac.uk/MSE3 /Topics/MSE-permeability.pdf, University of Edinburgh.

18. Lage, J. L., "The fundamental theory of flow through permeable media from Darcy to turbulence", Transport Phenomena in Porous Media, Editor: Ingham B. D. and Pop I., p1-30, 1998.

19. Kruger, E., "Die grundwasserbewegung", Internationale Mitteilungen Fur Bodenkunde", Vol.8, No.105, 1918. (cited in [18])

20. Hazen, A., "Some physical properties of sand and gravels with special reference to their use in filtration", Massachusetts State Board of Health, Twenty-fourth Annual

Report, p541, 1893.

21. Kozeny, J., "Ueber grundwasserbewegung, wasserkraft and wasserwirtschaft", Vol.22, No.67, 1927.

22. Dupuit, A. J. D. J., "Etudes theoriques et pratiques sur le movement des aux dans les canaux decouverts et a travers les terrains permeables", Victor Dalmont, Paris, 1863. (cited in [18])

23. Prony, R. de, "Recherches physico-mathematiques sur la theorie de eaux courants", Paris, 1804. (cited in [18])

24. Forchheimer, P., "Wasserbewegung durch boden", Zeitschrift des Vereines Deutscher Ingenieurs, Vol.45, p1736-1741, 1901.

25. Ward, J. C., "Turbulent flow in porous media", ASCE Journal of The Hydraulics Division, Vol.90, No.HY5, p1-12, 1964.

26. Beavers, G. S., Sparrow, E. M. and Rodenz, D. E., "Influence of bed size on the flow characteristics and porosity of randomly packed beds of spheres", Journal of Applied Mechanics, Vol.40, No.3, p655-660, 1973.

27. Antohe, B. V., Lage, J. L., Price, D. C. and Weber, R. M., "Experimental determination of permeability and inertia coefficients of mechanically compressed aluminum porous matrices", Journal of Fluids Engineering, Vol.119, No.2, p405-412, 1997.

28. Davis, P. A., Olague, N. E. and Goodrich, M. T., "Application of a validation strategy to Darcy's experiment", Advances in Water Resources, Vol.15, p175-180, 1992.

29. Boomsma, K. and Poulikakos, D., "The effects of compression and pore size

variations on the liquid flow characteristics in metal foams", Journal of Fluids Engineering, Vol.124, No.1, p263-272, 2002.

30. Diedericks, G. P. J. and Du Plessis, J. P., "Modeling of flow through homogeneous foams", Mathematical Engineering in Industry, Vol.6, No.3, p133-154, 1997.

31. Beckermann, C. and Viskanta, R., "Forced convection boundary layer flow and heat transfer along a flat plate embedded in a porous medium", International Journal of Heat and Mass Transfer, Vol.30, No.7, p1547-1551, 1987.

32. Tadrist, L. and Miscevic, M., "About the use of fibrous materials in compact heat exchangers", Experimental Thermal and Fluid Science, Vol.28, No.2, p193-199, 2004.

33. Paek, J. W., Kang, B. H., Kim, S. Y. and Hyun, J. M., "Effective thermal conductivity and permeability of aluminum foam materials", International Journal of Thermophysics, Vol.21, No.2, p453-464, 2000.

34. Innocentini, D.M. and Salvini Vania, "Prediction of ceramic foams permeability using Ergun's equation", Material Research (Sao Carlos, Brazil), Vol.2, No.4, p283-289, 1999.

35. Innocentini, D.M. and Victor, C., "Permeability of porous ceramic considering the Klinkenberg and inertial effects", Journal of the American Ceramic Society, Vol.84, No.5, p941-944, 2001.

36. Du Plessis P., "Pressure drop prediction for flow through high porosity metallic foams", Chemical Engineering Science, Vol.49, No.21, p3545-3553, 1994.

37. Fourie, J. G. and Du Plessis, P., "Pressure drop modeling in cellular metallic foams", Chemical Engineering Science, Vol.57, No.14, p2781-2789, 2002.

38. Boomsma, K., Poulikakos, D. and Ventikos, Y., "Simulations of flow through open cell metal foams using an idealized periodic cell structure", International Journal of Heat and Fluid Flow, Vol.24, No.6, p825-834, 2003.

39. Despois, J. F. and Mortensen, A., "Permeability of open-pore microcellular materials", Acta Materialia, Vol.53, No.5, p1381-1388, 2005.

40. Fand, R. M., Kim, B. Y. K., Lam, A. C. C. and Phan, R. T., "Resistance to the flow of fluid through Simple and complex porous media whose matrices are composed of randomly packed spheres", ASME Journal of Fluids Engineering, Vol.109, No.3, p268-274, 1987.

41. Innocentini, D.M., Salvini, V. R., Pandolfelli, V. C. and Coury, J. R., "The permeability ceramic foams", American Ceramic Society Bulletin, Vol.78, No.9, p78-84, 1999.

42. Innocentini, D. M., Antunes, W. L., Baumgartner, J. B., Seville, J. P. K. and Coury, J. R., "Permeability of ceramic membranes to gas flow", Materials Science Forum, Vol.299-300, No.5, p19-28, 1999.

43. Rumer, R. R. and Drinker, P., "Resistance to laminar flow through porous media", Journal of Hydraulic Div., American Society of Civil Engineers, Vol.89, No.6, p193, 1966.

44. Dullien, F. A. L., "Porous media: fluid transport and pore structures", Academic Press, New York, p180-190, 1979.

45. Carman, P. C., "The determination of the specific surface area of powder I", Journal of the Society of Chemical Industry, Vol.57, p225-234, 1938.

46. Rumpf, H. and Gupte, A. R., "Einfusse und korngrossenverteilung in

widerstansdesetz der porenstromung", Chemie-Ing. Techn., Vol.43, p367-375, 1971.

47. Happel, J and Brenner, H., **"**Low Reynolds number hydrodynamics: with special applications to particulate media", Englewood Cliffs, N.J., Prentice-Hall, p553, 1965.

48. Neale, G. H. and Nader, W. K., "Prediction of transport process within porous media: creeping flow relative to a fixed swarm of spherical particles", American Institute of Chemical Engineers, Vol.20, No.3, p530-538, 1974.

49. Brinkman, H. C., "Problems of fluid flow through swarms of particles and through macromolecules in solution", Research, London, Vol.2, p190-194, 1949.

50. Marshall, H., Sahraoui, M. and Kaviany, M., "An improved analytic solution for analysis of particle trajectories in fibrous, two dimensional filters", Physics of Fluids, Vol.6, No.2, p507-520, 1994.

51. Lefebvre, L.P., Gauthier, M., Bureau, M.N., LeRoux, M., Panneton, R. and Pilon, D., "Properties of nickel foams having different pore size distributions and densities", METFOAM conference, Berlin, Germany, June 2003.

52. ReceMat, "ReceMat metal foam: extremely porous material; ReceMat metal foam: flame arresters", ReceMat International, 2002.